STUDY OF CYLINDRICAL DIELECTRIC RESONATOR IN $TM_{01\delta}$ MODE AND IT'S APPLICATIONS TO MICROWAVE FILTERS

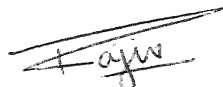EE - 1998 - M - DHI - STU

Entered in System

th
8.5.98

Ash
8.5.98

CERTIFICATE

This is to certify that the present M. Tech Thesis work entitled **Study of Dielectric Resonator in** $TM_{01\delta}$ **Mode and It's Applications to Microwave Filters,** *has been carried out by* **Major Sandeep Dhingra,** *under our supervision and it has not been submitted elsewhere for a degree.*

Rajiv Kumar Shukla
Research Engineer
COMDEV PHASE GROUP
PDL I.I.T.K. R&D Cell
Indian Institute of Technology
Kanpur
23 February 1998

Dr. Animesh Biswas
Associate Professor
Deptt. of Electrical Engg.
Indian Institute of Technology
Kanpur
23 February 1998

Abstract

In this thesis, a comprehensive study on *Dielectric Resonator* operating in $TM_{01\delta}$ mode, kept in various types of environments, has been done. The analysis presented here, is applicable to Isolated DR, DR post, DR in a cavity, DR in cylindrical metal waveguide below cut-off, suspended substrate etc. Various parameters, required for the design of microwave circuits including DR for millimeteric wave applications, have been studied and analytical formulations have been developed for them. The resonance frequency of a cylindrical DR for $TM_{01\delta}$ mode, is calculated using Dielectric Waveguide Model (DWM), and some modifications over it. The fields, energy distribution in all the regions of the structure are obtained. Q-factor has been found using the basic definition of Q, based on losses and energy relations. Inter-Resonator coupling between two identical DRs for edge coupled and broad-side coupled cases have been found, using electric dipole model having capacitive coupling.

Results obtained in this thesis, are in good agreement with the published results, where-ever available.

ACKNOWLEDGEMENT

Contents

...

List of Figures

List of Tables

Chapter 1

Introduction

1.1   Introduction

In the present age of miniaturisation of microwave components and their applications in millimeteric wave ranges, 'Dielectric Resonators' have found a prominent place, due to their spectacular properties of small size, high Q, temperature stability, high dielectric constant etc. [1], and by now these are so well known that it does not need a basic introduction. More basic details can be found in [1], [2], [3], [4].

Numerous analysis and synthesis methods are existing in various references [2], for characterisation of DRs, like Dielectric Waveguide Model (DWM), Mode matching, Integral equations and Green's function method, Finite element method (FEM), Finite difference time domain (FDTD) method etc. Almost all of these methods are of rigorous nature and are computation extensive. Also, ironically, most of these are dealing with only DRs excited in $TE_{0\gamma\delta}$ mode, being generally the dominant mode, and thus $TM_{0\gamma\delta}$ mode has been forsaken.

Off-late, with the increasing popularity of DR operating in $TM_{0\gamma\delta}$

mode in various applications like microwave filter design etc, it's analysis and characterisation has become a challenging task and only a few researchers have worked in this field so far. This thesis studies the circuit properties of DR operating in $TM_{01\delta}$ mode and presents a simple approximate method, which gives reasonably good results in determination of resonance frequency, energy distribution, Q-factor and coupling between two adjacent DRs in various environments and it's applications into design of an efficient microwave filter.

1.2   Subscript Notation

The modes of the dielectric resonators are denoted by HEM_{mnp} modes. Here first two subscripts denote the dielectric waveguide modes. For $m = 0$ (i.e. circular symmetry), the fields are split into transverse electric to z (TE to z) and transverse magnetic to z (TM to z) fields, completely independent of each other and with no ϕ-variation. For all $m > 0$, the fields are hybrid, or HEM, having both TE and TM parts.

The third subscript p denotes an integer number of half wavelength variations of the field, as a function of co-ordinate z. The notation $TE_{01\delta}$ or $TM_{01\delta}$, denotes lowest circular symmetric mode of that category (TE or TM) (with fields having no variation in ϕ direction), having field variations of less than one half-wavelength variation within the resonator length (i.e. height of a DR disc). δ therefore signifies a non-integer number, smaller than unity.

1.3   Organisation of Thesis

This thesis has been devided into seven chapters. Chapter2 discusses the DWM method for calculating resonance frequency, field distributions and coupling between two adjascent DRs in $TM_{01\delta}$ mode. Chapter3 presents the electric and magnetic energy distributions in all the regions of the DR's environment. In chapter4, the Q-factor of DR in various environments, has been presented. Chapter5 presents the analysis of DR in a generalised structure and determination of inter-resonator coupling. Chapter6 gives the design of a filter using DR in $TM_{01\delta}$ mode. Following this chapter comes the conclusion and future scope of these studies.

Chapter 2

Calculation of Resonance Frequency

2.1 Methods of Analysis

A number of techniques for analysis of dielectric resonators have been reported. Most of these are rigorous analysis methods, which are very complicated and computation extensive. Some of these are Mode Matching Technique, Method of Moments, Finite Element Method (FEM), Integral Equations and Green's Function techniques, Finite Difference Time Domain (FDTD) etc. Amongst the approximate analysis techniques, Dielectric Waveguide Model (DWM) is comparatively simple and takes reasonably less computation time. In most of the published literatures on these techniques, the analysis for only $TE_{01\delta}$ mode has been discussed, being most popular mode for various Microwave applications. However off-late, it has been shown that $TM_{01\delta}$ mode of dielectric resonator also shows very interesting properties. Therefore, now the attention has been diverted to the analysis of this mode which was forsaked earlier. In this thesis we have used the DWM method for the analysis of $TM_{01\delta}$ mode of dielectric resonator. A

similar analysis for $TE_{01\delta}$ mode, has already been presented in [6].

2.2 Dielectric Waveguide Model (DWM) Method

In DWM method, a dielectric resonator is considered as the dual of a metallic cavity. The DWM method is similar to Itoh's method [4], except in field expressions selected for axial electric field (E_z). As a truncated hollow waveguide becomes a resonant cavity, in the same way the truncated dielectric rod waveguide becomes a dielectric resonator. For circular symmetric configurations, suitable field expressions can be found for axial field components (E_z and H_z), from the knowledge of field analysis for dielectric rod waveguide. When we apply proper boundary conditions these field expressions give characteristic equation, the solution of which gives the resonance frequency.

2.2.1 Maxwell's Equations for TM_{0n} Case

For a source free, isotropic and homogeneous medium, the fundamental Maxwell's equations can be written as:-

$$\nabla \times \vec{E} = -j\omega\mu\vec{H}$$
$$\nabla \times \vec{H} = j\omega\epsilon\vec{E}$$
$$\nabla \cdot \vec{E} = 0$$
$$\nabla \cdot \vec{H} = 0 \qquad (2.1)$$

From the equations (2.1) we can easily find the well known vector Helmholtz equation :-

$$\nabla^2\vec{E} + k^2\vec{E} = 0$$
$$\nabla^2\vec{H} + k^2\vec{H} = 0 \qquad (2.2)$$

where k is called the wave number of the medium and in general, it is a complex quantity. For a dielectric medium of relative dielectric constant ϵ_r, the wave number k is given by :-

$$k^2 = k_0^2 \epsilon_r \qquad (2.3)$$

where, $k_0 = 2\pi f_0 \sqrt{\mu_0 \epsilon_0}$ and f_0 is the resonance frequency. To obtain the fields in all the regions of a structure, it is convenient to start from the axial component of the electric or magnetic field. Other field components can be obtained from this axial field with the help of Maxwell's equations. For TM to z mode (i.e. $H_z = 0$), we can start from the axial electric field i.e. E_z. Then vector Helmholtz equation (2.2) reduces to scalar form as follows :-

$$\nabla^2 E_z + k^2 E_z = 0 \qquad (2.4)$$

This equation can be solved by well known separation of variables method. The field components for TM to z circular symmetrical case ($\partial/\partial\phi = 0$) are expressed as [2] :-

$$
\begin{aligned}
E_z &= chosen & H_z &= 0 \\
E_r &= \frac{1}{\nu^2}\frac{\partial^2 E_z}{\partial z \partial r} & H_r &= 0 \\
E_\phi &= 0 & H_\phi &= -\frac{j\omega\epsilon}{\nu^2}\frac{\partial E_z}{\partial r}
\end{aligned}
\qquad (2.5)
$$

Here, ν is defined as the radial wave number, and in general is given by :-

$$\nu^2 = \pm (k^2 - k_z^2) \qquad (2.6)$$

where, k_z is the axial wave number.

2.2.2 Field Distributions in the Resonator

The cross sectional view of cylindrical resonator placed coaxially in a circular metal waveguide cavity is shown in Fig 2.1. For the generallity of the analysis, the top and bottom circular plates of the circular waveguide cavity, can be considered in four possible combinations as follows :-

1. Top and Bottom circular plates to be PEC

2. Top and Bottom circular plates to be PMC

3. Top plate PEC and Bottom plate to be PMC

4. Top plate PMC and Bottom plate to be PEC

The resonator material is assumed to be a perfect dielectric characterised by the real scalar relative permittivity ϵ_d and the real scalar permeability μ ($= \mu_0$). To simplify the analysis, this composite structure is devided into six regions with a different set of field components. Here the proper choice of E_z in different regions, depends on the requirements imposed by physical geometry and the analyticity of the field at the origin. It also should satisfy the wave equation (2.4). Inside the resonator, E_z should represent standing wave in z direction, and wave number $\nu = k_r$ should be real to fulfill the requirement of DR as a energy storing element. The solution of equation (2.4) in cylindrical co-ordinates using method of separation of variables with above mentioned conditions gives the following form of expressions for E_z in Region 1 :-

$$E_{z1} = \{\cos(\beta_1 z) + B_1 \sin(\beta_1 z)\} \, J_0(k_r r) \tag{2.7}$$

where J_0 is the Bessel function of the first kind and zero order, and k_r is related to axial wave number β_1 by separation relation :-

$$k_r^2 + \beta_1^2 = \epsilon_d k_0^2 \tag{2.8}$$

7

Outside the resonator E_z should be axially symmetric, but decaying in
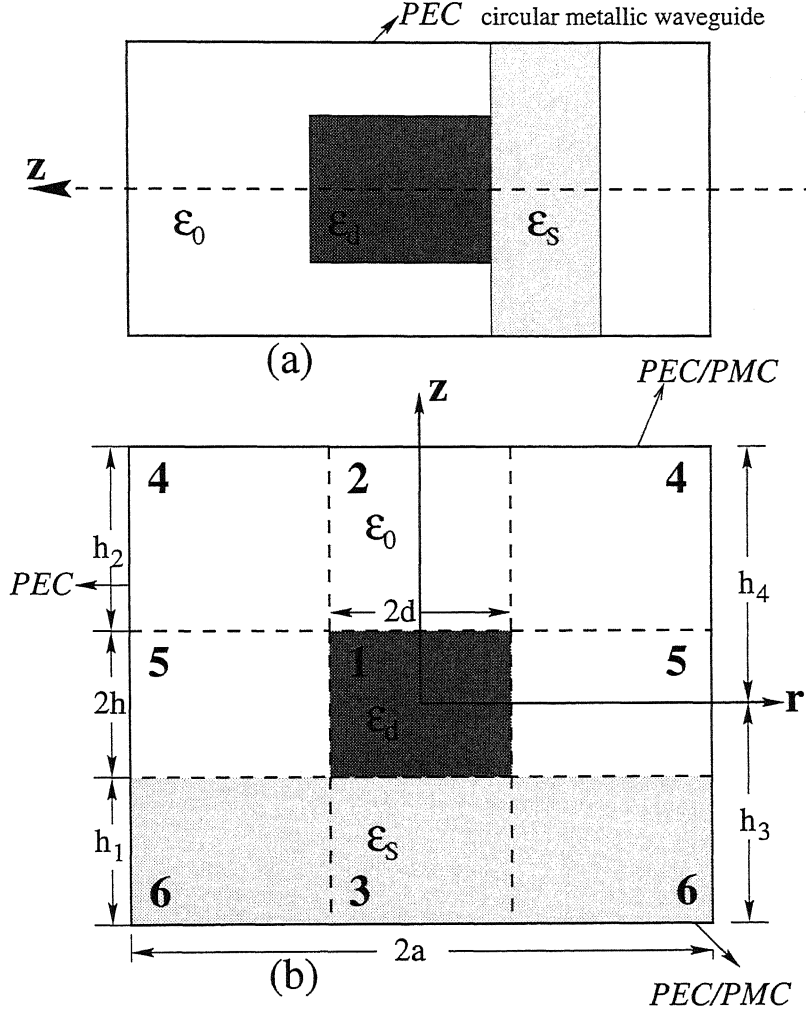
Figure 2.1: (a) Cylindrical dielectric resonator in a cylindrical waveguide. (b) Cross-sectional view of DR in a cavity

nature in the direction away from the resonator, for confirming the maximum energy storage inside the resonator. This decay in radial direction can be represented by modified bessel functions, therefore, outside the resonator (in the radial direction) the radial wavenumber becomes imaginary. Finally, tangential electric fields should vanish at the PEC surfaces and tangential magnetic fields should vanish at the PMC surfaces. Again solving equation (2.4) with these conditions, E_z in the rest of the regions (2, 3, 4, 5, 6) can

be written as follows. (Note :- Upper term inside the square braces [ ] is for PEC surface at that end of the cavity and lower term is for PMC surface.)

$$E_{z2} = B_2 \begin{bmatrix} \cosh\{\alpha_a(z - h_4)\} \\ -\sinh\{\alpha_a(z - h_4)\} \end{bmatrix} e^{-\alpha_a h_4} \; J_0(k_r r)$$

$$E_{z3} = B_3 \begin{bmatrix} \cosh\{\alpha_s(z + h_3)\} \\ \sinh\{\alpha_s(z + h_3)\} \end{bmatrix} e^{-\alpha_s h_3} \; J_0(k_r r)$$

$$E_{z4} = B_5 \begin{bmatrix} \cosh\{\alpha_a(z - h_4)\} \\ -\sinh\{\alpha_a(z - h_4)\} \end{bmatrix} e^{-\alpha_a h_4} \; \{K_0(k_a r) - B I_0(k_a r)\}$$

$$E_{z5} = B_6 \; \{\cos(\beta_1 z) + B_1 \sin(\beta_1 z)\} \; \{K_0(k_a r) - B I_0(k_a r)\}$$

$$E_{z6} = B_7 \begin{bmatrix} \cosh\{\alpha_s(z + h_3)\} \\ \sinh\{\alpha_s(z + h_3)\} \end{bmatrix} e^{-\alpha_s h_3} \; \{K_0(k_a r) - B I_0(k_a r)\} \quad (2.9)$$

where,

$$B = K_0(k_a a)/I_0(k_a a) \qquad (2.10)$$

$I_n(x)$ and $K_n(x)$ are the modified bessel functions of the first and second kinds. The separation relations in these regions are :-

$$k_r^2 = k_0^2 + \alpha_a^2 \qquad (2.11)$$

$$k_r^2 = \epsilon_s k_0^2 + \alpha_s^2 \qquad (2.12)$$

$$k_a^2 = -k_0^2 - \alpha_a^2 \qquad (2.13)$$

$$k_a^2 = -k_0^2 + \beta_1^2 \qquad (2.14)$$

$$k_a^2 = -\epsilon_s k_0^2 - \alpha_s^2 \qquad (2.15)$$

The transverse field components in various regions are found by substituting (2.7) and (2.9) into (2.5), and are given as :-

Region 1

$$E_{r1} = -\frac{\beta_1}{k_r} \{B_1 \cos(\beta_1 z) - \sin(\beta_1 z)\} J_1(k_r r)$$

$$H_{\phi 1} = \frac{j\omega\epsilon_0\epsilon_d}{k_r} \{\cos(\beta_1 z) + B_1 \sin(\beta_1 z)\} J_1(k_r r) \qquad (2.16)$$

be written as follows. (Note :- Upper term inside the square braces [ ] is for PEC surface at that end of the cavity and lower term is for PMC surface.)

$$E_{z2} = B_2 \begin{bmatrix} \cosh\{\alpha_a(z - h_4)\} \\ -\sinh\{\alpha_a(z - h_4)\} \end{bmatrix} e^{-\alpha_a h_4} \; J_0(k_r r)$$

$$E_{z3} = B_3 \begin{bmatrix} \cosh\{\alpha_s(z + h_3)\} \\ \sinh\{\alpha_s(z + h_3)\} \end{bmatrix} e^{-\alpha_s h_3} \; J_0(k_r r)$$

$$E_{z4} = B_5 \begin{bmatrix} \cosh\{\alpha_a(z - h_4)\} \\ -\sinh\{\alpha_a(z - h_4)\} \end{bmatrix} e^{-\alpha_a h_4} \; \{K_0(k_a r) - B I_0(k_a r)\}$$

$$E_{z5} = B_6 \; \{\cos(\beta_1 z) + B_1 \sin(\beta_1 z)\} \; \{K_0(k_a r) - B I_0(k_a r)\}$$

$$E_{z6} = B_7 \begin{bmatrix} \cosh\{\alpha_s(z + h_3)\} \\ \sinh\{\alpha_s(z + h_3)\} \end{bmatrix} e^{-\alpha_s h_3} \; \{K_0(k_a r) - B I_0(k_a r)\} \quad (2.9)$$

where,

$$B = K_0(k_a a)/I_0(k_a a) \tag{2.10}$$

$I_n(x)$ and $K_n(x)$ are the modified bessel functions of the first and second kinds. The separation relations in these regions are :-

$$k_r^2 = k_0^2 + \alpha_a^2 \tag{2.11}$$

$$k_r^2 = \epsilon_s k_0^2 + \alpha_s^2 \tag{2.12}$$

$$k_a^2 = -k_0^2 - \alpha_a^2 \tag{2.13}$$

$$k_a^2 = -k_0^2 + \beta_1^2 \tag{2.14}$$

$$k_a^2 = -\epsilon_s k_0^2 - \alpha_s^2 \tag{2.15}$$

The transverse field components in various regions are found by substituting (2.7) and (2.9) into (2.5), and are given as :-

Region 1

$$E_{r1} = -\frac{\beta_1}{k_r} \{B_1 \cos(\beta_1 z) - \sin(\beta_1 z)\} J_1(k_r r)$$

$$H_{\phi 1} = \frac{j\omega\epsilon_0\epsilon_d}{k_r} \{\cos(\beta_1 z) + B_1 \sin(\beta_1 z)\} J_1(k_r r) \tag{2.16}$$

Region 2

$$E_{r2} = \frac{\alpha_a B_2}{k_r} \begin{bmatrix} -\sinh\{\alpha_a(z-h_4)\} \\ \cosh\{\alpha_a(z-h_4)\} \end{bmatrix} e^{-\alpha_a h_4} \, J_1(k_r r)$$

$$H_{\phi 2} = \frac{j\omega\epsilon_0 B_2}{k_r} \begin{bmatrix} \cosh\{\alpha_a(z-h_4)\} \\ -\sinh\{\alpha_a(z-h_4)\} \end{bmatrix} e^{-\alpha_a h_4} \, J_1(k_r r) \qquad (2.17)$$

Region 3

$$E_{r3} = \frac{\alpha_s B_3}{k_r} \begin{bmatrix} -\sinh\{\alpha_s(z+h_3)\} \\ -\cosh\{\alpha_s(z+h_3)\} \end{bmatrix} e^{-\alpha_s h_3} \, J_1(k_r r)$$

$$H_{\phi 3} = \frac{j\omega\epsilon_0\epsilon_s B_3}{k_r} \begin{bmatrix} \cosh\{\alpha_s(z+h_3)\} \\ \sinh\{\alpha_s(z+h_3)\} \end{bmatrix} e^{-\alpha_s h_3} \, J_1(k_r r) \qquad (2.18)$$

Region 4

$$E_{r4} = \frac{\alpha_a B_5}{k_a} \begin{bmatrix} \sinh\{\alpha_a(z-h_4)\} \\ -\cosh\{\alpha_a(z-h_4)\} \end{bmatrix} e^{-\alpha_a h_4} \, \{K_1(k_a r) + BI_1(k_a r)\}$$

$$H_{\phi 4} = \frac{j\omega\epsilon_0 B_5}{k_a} \begin{bmatrix} -\cosh\{\alpha_a(z-h_4)\} \\ \sinh\{\alpha_a(z-h_4)\} \end{bmatrix} e^{-\alpha_a h_4} \, \{K_1(k_a r) + BI_1(k_a r)\}$$

$$(2.19)$$

Region 5

$$E_{r5} = \frac{\beta_1 B_6}{k_a} \{B_1\cos(\beta_1 z) - \sin(\beta_1 z)\}\{K_1(k_a r) + BI_1(k_a r)\}$$

$$H_{\phi 5} = -\frac{j\omega\epsilon_0 B_6}{k_a} \{\cos(\beta_1 z) + B_1\sin(\beta_1 z)\}\{K_1(k_a r) + BI_1(k_a r)\} \quad (2.20)$$

Region 6

$$E_{r6} = \frac{\alpha_s B_7}{k_a} \begin{bmatrix} \sinh\{\alpha_s(z+h_3)\} \\ \cosh\{\alpha_s(z+h_3)\} \end{bmatrix} e^{-\alpha_s h_3} \, \{K_1(k_a r) + BI_1(k_a r)\}$$

$$H_{\phi 6} = -\frac{j\omega\epsilon_0\epsilon_s B_7}{k_a} \begin{bmatrix} \cosh\{\alpha_s(z+h_3)\} \\ \sinh\{\alpha_s(z+h_3)\} \end{bmatrix} e^{-\alpha_s h_3} \, \{K_1(k_a r) + BI_1(k_a r)\}$$

$$(2.21)$$

The values of unknown coefficients B_{is}, can be evalvated by applying the boundary conditions at the interfaces of two adjacent regions, and are given at Appendix A.

2.2.3 Resonance Frequency (f_0)

If k_r and β_1 are known, then the resonance frequency f_0 can be calculated from equation (2.8). The concept of dielectric waveguide model (DWM) is used for determination of k_r and β_1 [7]. These are determined as follows.

2.2.4 Determination of k_r

The resonator is first assumed to extend to infinity in z direction (Fig 2.2 (a)) for determining k_r. We assume that this infinite dielectric cylinder carries $TM_{01\delta}$ mode as the propagating mode, and that k_r is radial wave number for this cylinder, for $r \leq d$. Applying the continuity condition for tangential electric field and magnetic field components at the common boundary of Region 1 and Region 5, at $r = d$, gives the following characteristic equation:-

$$\frac{J_0(k_r d)}{\{K_0(k_a d) - BI_0(k_a d)\}} + \frac{k_a \epsilon_d}{k_r} \frac{J_1(k_r d)}{\{K_1(k_a d) + BI_1(k_a d)\}} = 0 \qquad (2.22)$$

Radial wavenumber k_r is related to k_a by :-

$$k_a = \sqrt{(\epsilon_d - 1.0)k_0^2 - k_r^2} \qquad (2.23)$$

k_r and k_a can be computed by solving equation (2.22) and (2.23).

2.2.5 Determination of β_1

The structure of Fig 2.1(b) is assumed to be a radial double slab waveguide (Fig 2.2(b)), alongwhich the $TM_{01\delta}$ guide mode is propagating. In other words it is assumed that the axial wave number β_1 is the same as that of a double layer slab guide structure, obtained by extending the resonator to infinity in the radial direction. When we apply the boundary

(a) for k_r (b) for β_1
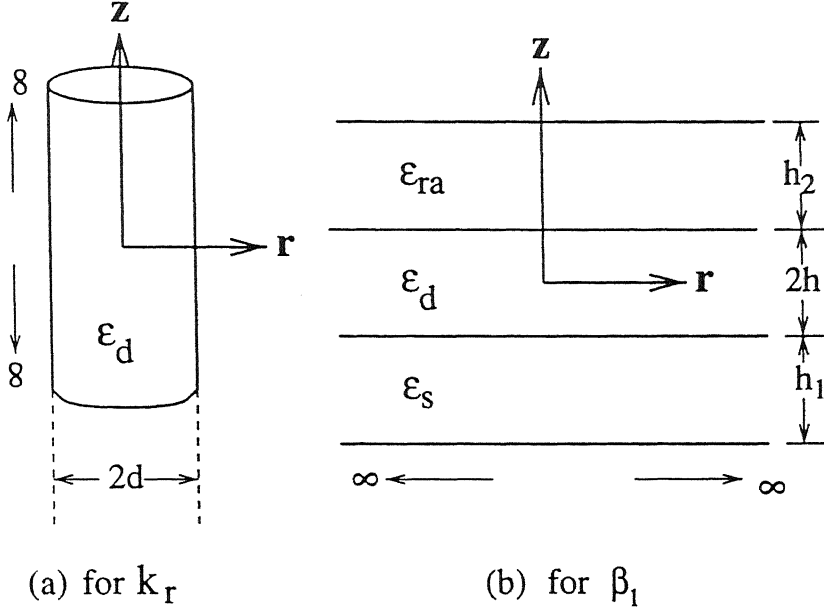
Figure 2.2: Determination of k_r and β_1 [7]

conditions at the interfaces of these regions at $z = \pm h$, $0 \leq r \leq d$, we get one more trancendental equation given by :-

$$\frac{m_1 \tan(\beta_1 h) - 1.0}{m_1 + \tan(\beta_1 h)} - \frac{1.0 - m_2 \tan(\beta_1 h)}{m_2 + \tan(\beta_1 h)} = 0 \qquad (2.24)$$

where,

$$m_1 = \frac{\beta_1}{\epsilon_d \alpha_a} \left[\begin{array}{c} \coth(\alpha_a h_2) \\ \tanh(\alpha_a h_2) \end{array} \right] \qquad (2.25)$$

$$m_2 = \frac{\beta_1 \epsilon_s}{\epsilon_d \alpha_s} \left[\begin{array}{c} \coth(\alpha_s h_1) \\ \tanh(\alpha_s h_1) \end{array} \right] \qquad (2.26)$$

We get the value of k_r by solving trancendental equation (2.22) in conjunction with equation (2.23). Then we can solve equation (2.24) for resonance frequency f_0 for specified height of the DR (i.e. $2h$), after substituting the values of β_1, α_a, α_s from the separation relations (2.11) - (2.13).

2.2.6 EDC Approach

As it will be shown in the next section, the DWM method gives slightly higher results for the resonance frequency f_0. This error is very large when a PEC surface is very close to the circular face of the DR. Mongia [7] suggested effective dielectric constant approach (EDC) for calculating the radial wavenumber (k_r) for $TE_{01\delta}$ mode, which increases the accuracy of DWM method. As per this approach radial wavenumber k_r is assumed to be the wavenumber of an infinitely long cylindrical waveguide having same radius as that of DR, but having a dielectric constant ϵ_{eff}, which is less than that of the resonator. The relations used in [7] are :-

$$k_a = \left\{ (\epsilon_{eff} - 1.0) k_0^2 - k_r^2 \right\}^{1/2} \tag{2.27}$$

where,

$$\epsilon_{eff} = (\epsilon_{effa} + \epsilon_{effb})/2.0$$
$$\epsilon_{effa} = \begin{cases} \epsilon_d - (\epsilon_d - \epsilon_{eff0}) h_1/d & if(h_1 < d) \\ \epsilon_{eff0} & otherwise \end{cases}$$
$$\epsilon_{effb} = \begin{cases} \epsilon_d - (\epsilon_d - \epsilon_{eff0}) h_2/d & if(h_2 < d) \\ \epsilon_{eff0} & otherwise \end{cases}$$
$$\epsilon_{eff0} = k_r^2(\epsilon_d)/k_0^2$$

2.2.7 Numerical Implementation

Above analysis is very general in nature, and it is applicable for isolated DR $(2a \to \infty, h1 \to \infty, h2 \to \infty)$, dielectric post having top and bottom circular plates PEC $(h1 \approx 0, h2 \approx 0)$, as well as DR in MIC environment. Based on this analysis, a menu driven software package (DRTM6) has been developed for the calculation of resonance frequency for top and bottom circular plates (Fig 2.1) being PEC or PMC. The structural parameters including the dimensions of DR, are assumed to be known. In this program the

computation is started by finding the root of equation (2.22) using Newton Ralphson method with following initial approximate value of $k_r(\epsilon_d)$[7] :-

$$k_r(\epsilon_d) \;=\; \left[0.951\chi_{01} + 0.222\left\{(\epsilon_d - 1)(k_0 d)^2 - 0.951\chi_{01}^2\right\}^{1/2}\right]/d \quad (2.28)$$

where, $\chi_{01} = 2.405$, and is the first root of the equation $J_0(x) = 0$. Other eigen values and the resonance frequency of the resonator can be computed, when k_r and k_a are determined. Repeated iterative procedure is used to get the value of f_0 within tolerable accuracy.

2.2.8   Numerical Results

DR Post

The results obtained for f_0 of a DR post (top and bottom circular faces of DR covered with PEC), are presented in Table 2.1 alongwith the published results of rigorous analysis methods of mode matching technique [8] and Finite Element Method (FEM) [9]. A comparison of resonance frequencies obtained by present method, and that of rigorous analysis method shows good agreement.

Isolated DR

The results obtained for f_0 of an isolated DR, are presented in Table 2.2 alongwith the published results and it is found that the present DWM method gives very close results on slightly higher side, to those published for rigorous methods and EDC method gives very close results on slightly lower side of the published results. The error is within 2% and it further reduces as value of ϵ_d increases.

Table 2.1: Comparison of Resonance Frequencies from DWM method, with published data for DR post

$h_1 = h_2 = 1.0 \times 10^{-5} mm$, $\epsilon_d = 37.6$, $\epsilon_s = 1.0$, $d = 10.0076mm$, $a = 12.7mm$

2h	Resonance Frequencies (f_0) GHz		
	f_0 [8]	f_0 [9]	f_0
(mm)	Mode Matching	FEM	Present
13.97	3.363	3.38 [15]	3.389
11.55	3.582	3.613	3.6109
10.0076	3.802	3.824	3.8205
8.95	4.013	4.020	4.0165
8.17	4.189	4.205	4.2016
7.56	4.403	4.381	4.3790
7.076	4.550	4.5501	4.5466
6.67	4.710	4.713	4.709

Table 2.2: Comparison of Resonance Frequencies from DWM and EDC methods, with published data for isolated DR

$h_1 = h_2 = 100mm$, $\epsilon_s = 1.0$, $a = 100mm$

ϵ_d	2h	d	Resonance frequencies (f_0) GHz		
	(mm)		f_0 [Reported]	f_0 Present (DWM)	f_0 Present (EDC)
19.5	8.53	4.265	9.44 [10]	9.603	9.375
38.0	4.60	5.250	7.5384 [11]	7.643	7.415
-do-	-do-	- do -	7.524/7.6 [12]	-do-	-do-
-do-	-do-	- do -	7.6 [13]	-do-	-do-
38.0	5.62	6.415	6.1328 [14]	6.256	6.069
79.7	4.51	5.145	5.4072 [14]	5.419	5.318

DR in a Cavity having PMC walls

The results are obtained for f_0 of a DR placed in a cylindrical cavity, having top and bottom circular plates made of PMC, and are shown in Fig 2.3. These have been compared with the results published in [16] and they are found to be in close agreement. The error slowly increases as the PMC walls are taken away from the DR. However, the EDC method gives slightly low but more closer results.
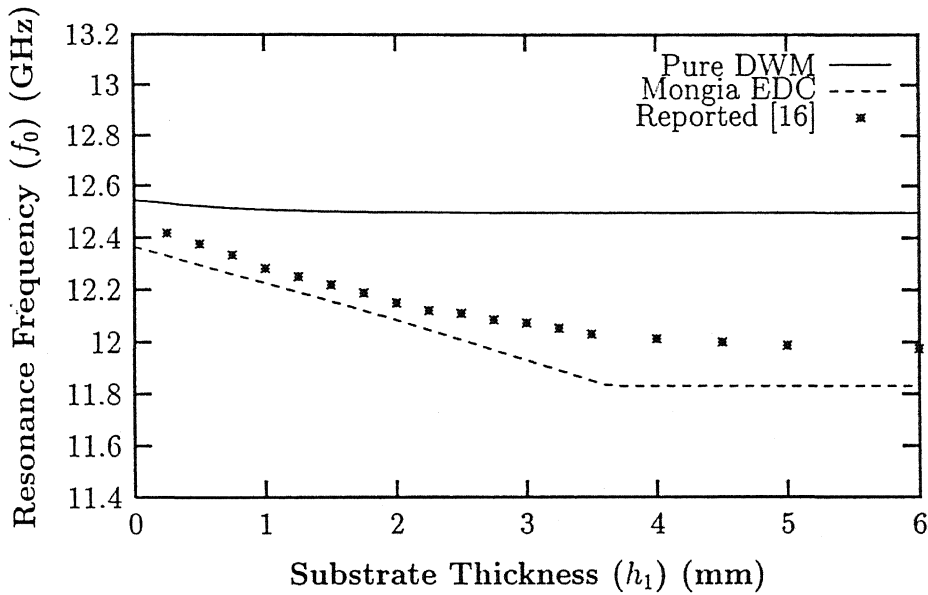
h_2=15mm, ϵ_d=24, ϵ_s=1, d=3.635mm, a=5.45mm, 2h=4.04mm

Figure 2.3: Comparison with published data for DR in a cavity with top and bottom walls PMC

DR in a Cavity having PEC walls

The results are obtained for f_0 of a DR placed in a cylindrical PEC cavity and are shown in Fig 2.4. These have been compared with the results published in [16], and it was found that the present DWM method gives very high resonance frequency, especially for close distance of PEC circular plates.

The error reduces as the PEC walls are taken away from the DR surface. The EDC method also somewhat tends to fail for close proximity of PEC walls and thereafter it gives a feel of fall in resonance frequency with increase in wall distance, till it saturates for an isolated DR case. The reason for such a
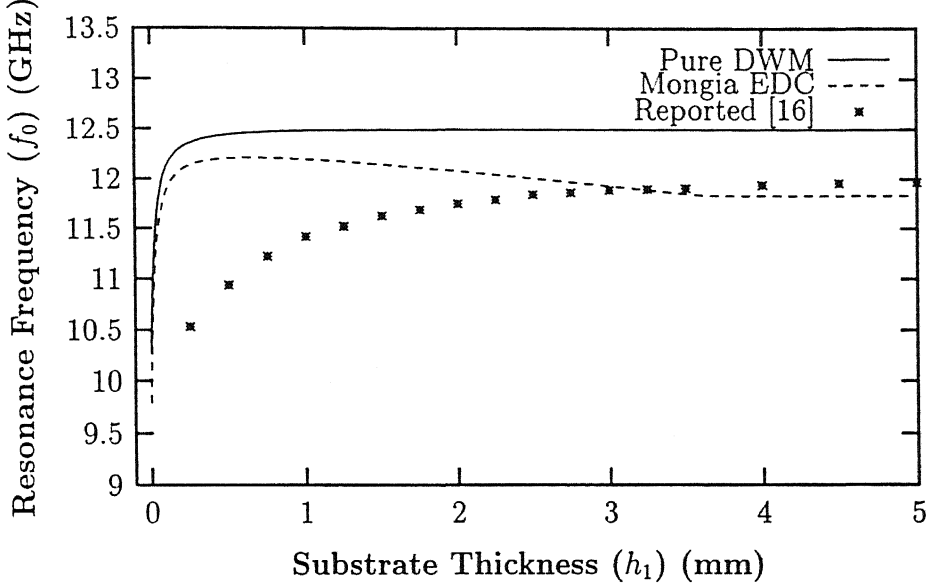
h_2=15mm, ϵ_d=24, ϵ_s=1, d=3.635mm, a=5.45mm, 2h=4.04mm

Figure 2.4: Comparison of results from pure DWM and EDC methods, with published data for DR in a PEC cavity.

high results obtained from DWM method are analysed to be happening due to mismatching of the fields in the outer regions of the cavity e.g. Region 2-4, 3-6, 4-5, 5-6. Therefore for PEC cavity we had tried to use the modified DWM method.

2.3   Modified DWM Method

If we match the boudary conditions for continuity of tangential fields at $r = d$, $h \leq z \leq h_4$ and $-h \leq z \leq -h_3$ in Fig 2.1 then we find a new

trancendental equation as :-

$$\frac{J_0(k_r d)}{\{K_0(k_a d) - BI_0(k_a d)\}} + \frac{k_a}{k_r} \frac{J_1(k_r d)}{\{K_1(k_a d) + BI_1(k_a d)\}} = 0 \qquad (2.29)$$

Similarly, on matching the tangential fields at $z = \pm h$, $d \le r \le a$ we again find a new trancendental equation as follows :-

$$\frac{m_1' \tan(\beta_1 h) - 1.0}{m_1' + \tan(\beta_1 h)} - \frac{1.0 - m_2' \tan(\beta_1 h)}{m_2' + \tan(\beta_1 h)} = 0 \qquad (2.30)$$

where,

$$m_1' = \frac{\beta_1}{\alpha_a} \left[\begin{array}{c} \coth(\alpha_a h_2) \\ \tanh(\alpha_a h_2) \end{array} \right] \qquad (2.31)$$

$$m_2' = \frac{\beta_1 \epsilon_s}{\alpha_s} \left[\begin{array}{c} \coth(\alpha_s h_1) \\ \tanh(\alpha_s h_1) \end{array} \right] \qquad (2.32)$$

In order to include the effects of these additional trancendental equations (due to fields in the outer regions) we modify the trancendental equation to be solved to determine the resonance frequency, by combining equation (2.24) and (2.30), as follows :-

$$\left(\frac{m_1 \tan(\beta_1 h) - 1}{m_1 + \tan(\beta_1 h)} - \frac{1 - m_2 \tan(\beta_1 h)}{m_2 + \tan(\beta_1 h)} \right) \cdot$$
$$\left(\frac{m_1' \tan(\beta_1 h) - 1}{m_1' + \tan(\beta_1 h)} - \frac{1 - m_2' \tan(\beta_1 h)}{m_2' + \tan(\beta_1 h)} \right) = 0 \quad (2.33)$$

Therefore, for a particular position of PEC walls either first term is zero, or second term is zero, or both are individually zero. The effect of equation (2.29) has however been neglected, as any change in this equation, changes all the results drastically.

2.3.1   Numerical Implementation

Now, solving equation (2.22) in conjunction with equation (2.23) for radial wavenumber k_r, and equation (2.33) in conjunction with equation

(2.25), (2.26), (2.31) and (2.32), we can find the resonance frequency for a DR placed in a PEC cavity, as done in section 2.2.

2.3.2   Results for DR in a PEC Cavity

The results are obtained for f_0 of a DR placed in a cylindrical PEC cavity, using modified DWM approach and are compared with that in [16] and it was found that the new resonance frequency is in close agreement, especially for very close distances of PEC from DR's flat surface, however the error increases slightly as the PEC wall is taken away from the DR, as shown in Fig 2.5.
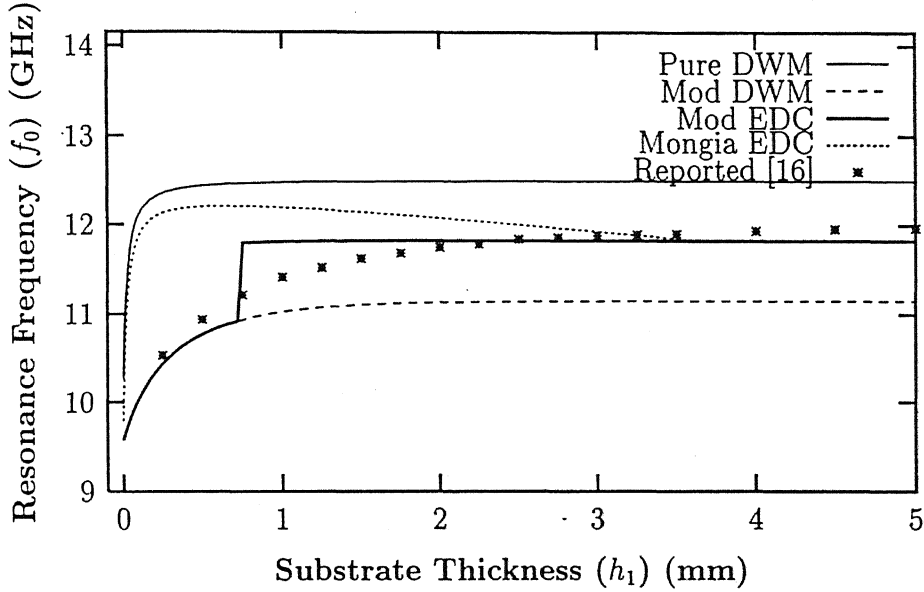
h_2=15mm, ϵ_d=24, ϵ_s=1, d=3.635mm, a=5.45mm, 2h=4.04mm

Figure 2.5: Comparison of results from different theories, with published data for DR in PEC cavity

2.4 Final Selection of Theory

On perusal of the results obtained from various theories used, it was decided to use Pure DWM or Pure EDC for the case of DR in a cavity having top and bottom walls PMC. However, for DR in PEC cavity, upto a distance of $0 < h_1/d < 0.2$ and/or $0 < h_2/d < 0.2$, modified DWM is used and thereafter we switchover to the modified EDC i.e. using ϵ_{eff0} for $h_1/d > 0.2$ and/or $h_2/d > 0.2$, for calculation of radial wavenumber k_r. The results of this, are shown in Figure 2.6, in which the sudden jump in the variation is at the place where theory used is switched from Modified DWM to Modified EDC.
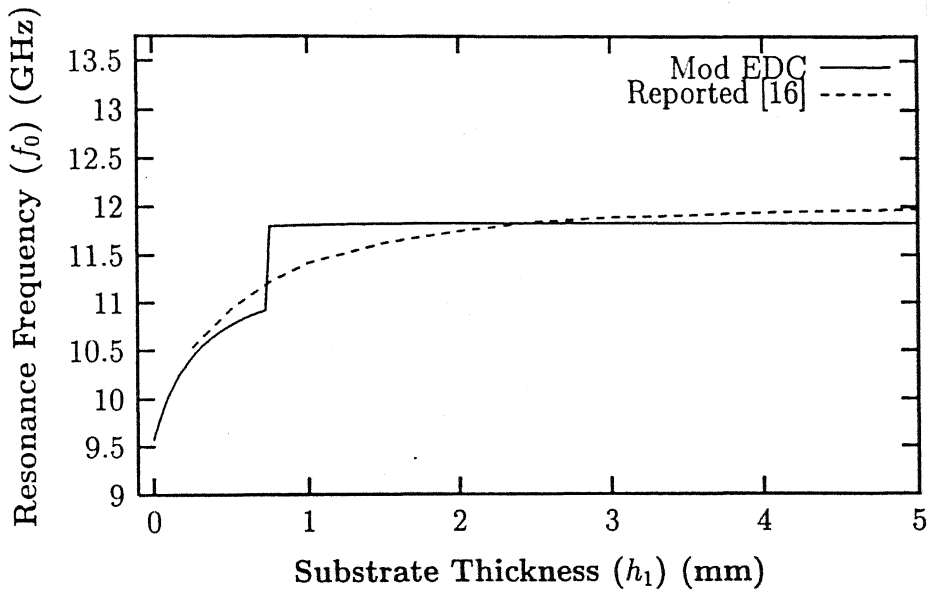
h_2=15mm, ϵ_d=24, ϵ_s=1, d=3.635mm, a=5.45mm, 2h=4.04mm

Figure 2.6: Variation of Resonance frequency with h_1 using modified method.

2.5 Effect of Design Parameters on f_0

Various electrical and physical parameters of the circuit, which are under control of the designer at the time of fabrication of the circuit, may change the resonance frequency of the DR in the cavity. Informations presented in the Figs 2.6 to 2.10, shows the impact of these control variables over resonance frequency f_0.

$h_1=6.98466$mm, $h_2=12.318394$mm, $\epsilon_s=1$, d=8.88957mm,

a=12.69937mm, h=6.0957mm
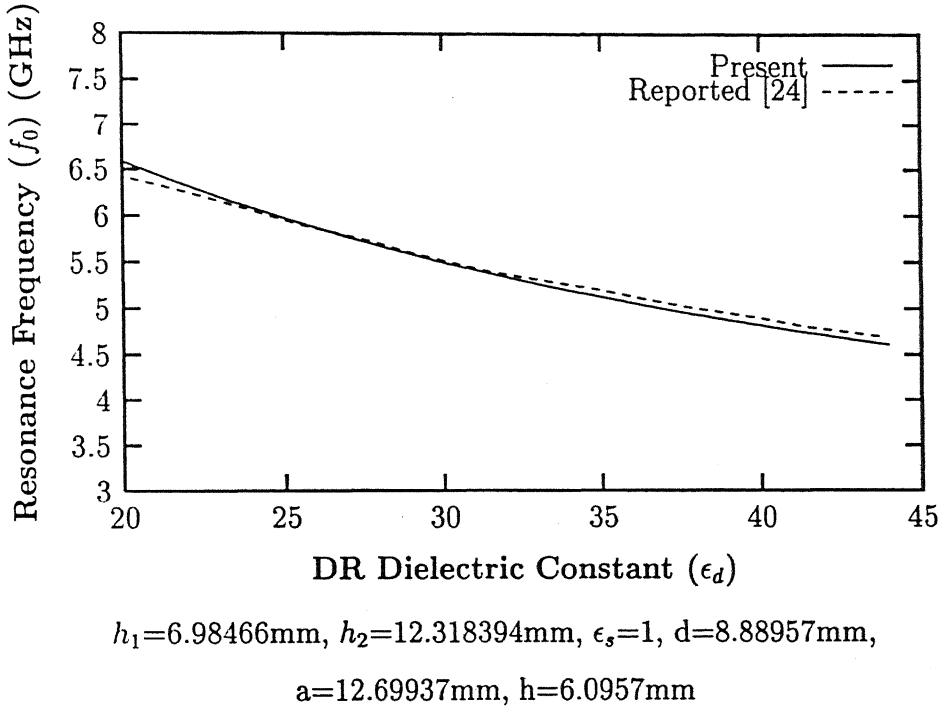
Figure 2.7: Variation of Resonance frequency with dielectric constant of DR (ϵ_d)

2.5.1 DR in a PEC cavity

The effects of separation (h_2) between top PEC plate and the top surface of the DR, over f_0, are similar as that of h_1 as shown in Fig 2.6. Variations of resonance frequency with h_2 can be explained by the cavity

perterbation theory i.e. when a metal wall of a resonant cavity is moved inwards, the resonance frequency of the cavity will increase if the stored energy of the displaced fields, is predominantly electric, which is the case with $TM_{01\delta}$ mode.
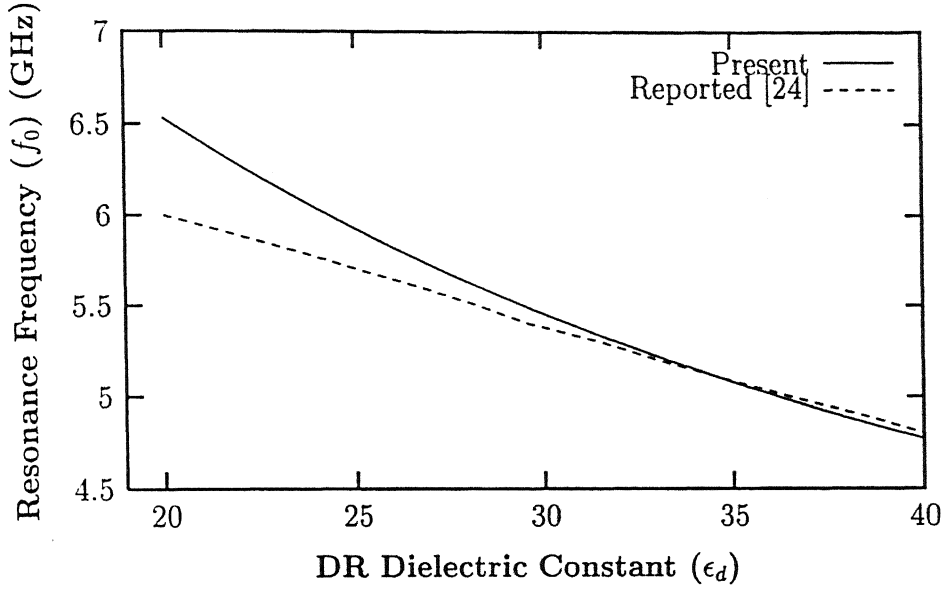
$h_1 = 1.0 \times 10^{-5}$, $h_2 = 20.319$mm, $\epsilon_s = 1$, d=6.34969mm, a=12.69937mm, 2h=5.07975mm

Figure 2.8: Variation of Resonance frequency with dielectric constant of DR (ϵ_d)

Fig 2.7 shows the effects of the dielectric constant (ϵ_d) of the DR, on it's resonance frequency. We find that the resonance frequency decreases with the increase in the value of ϵ_d. Hence the material of the DR should be temperature stable to get stable resonance frequency. Here, modified EDC part of the theory has come into play and gives close results to those reported in [24]. Fig 2.8 also shows the variation of ϵ_d with f_0 but for a DR placed on the PEC surface. Here, modified DWM part of theory has come into play and gives very close results to those in [24]. Fig 2.9 shows the effects of substrate dielectric constant (ϵ_s) over the resonance frequency. It is found that the

22
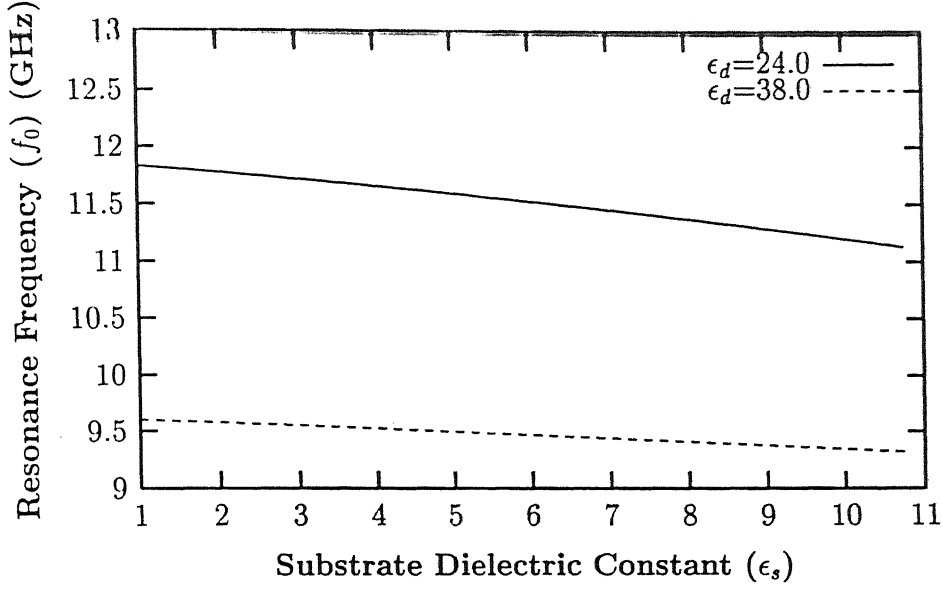
$h_2 = h_1$=3mm, d=3.635mm, a=5.45mm, 2h=4.04mm

Figure 2.9: Variation of Resonance frequency with dielectric constant of substrate (ϵ_s)

resonance frequency decreases with the increase in the substrate dielectric constant. Fig 2.10 shows the effects of height of the DR $(2h)$ over f_0, since the DR height can also be used as a prime design parameter in excitation of a particular mode of the DR and achieving a particular resonance frequency. With increase in DR height the resonance frequency is found to be decreasing rapidly.

2.5.2   DR in a Cavity with PMC walls

The effects of separation (h_2) between top PMC plate and the top surface of the DR, over resonance frequency f_0, is found to be decreasing with the increase in the separation h_2, and is same as that of h_1 as shown in Fig 2.3. The variations of resonance frequency with the dielectric constant of the DR (ϵ_d), substrate dielectric constant (ϵ_s), DR height $(2h)$ are found
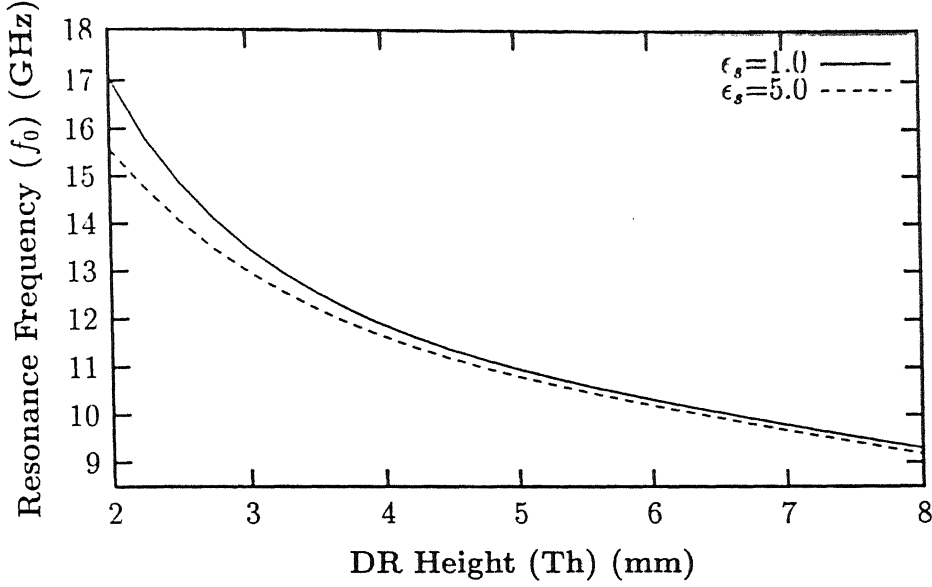
$$h_2 = h_1 = 3\text{mm}, \epsilon_d = 24, \text{d} = 3.635\text{mm}, \text{a} = 5.45\text{mm}$$

Figure 2.10: Variation of Resonance frequency with height of the DR ($2h$)

to be similar to the case of PEC cavity.

2.6 Coupling Between Two DRs

For the $TM_{01\delta}$ mode, coupled identical resonators placed in the configuration shown in Fig 2.11, inter-resonator coupling can be computed using the resonance frequencies for a DR placed in a PEC cavity (f_{sh}) and that of placed in a cavity having top and bottom circular plates to be PMC (f_{op}). Kobayashi *etal.* [16] has reported this method of computing the coupling coefficient. The calculated results show that $f_{op} > f_{sh}$, which is in contrast with the usual inductively coupled case for the $TE_{01\delta}$ mode in which $f_{sh} > f_{op}$. Cohn [3] had shown that the inter-resonator coupling is caused by an axial magnetic dipole for the $TE_{01\delta}$ mode. By analogy with this case, we expect that it is done by an axial electric dipole for the $TM_{01\delta}$ mode. Then we shall consider the capacitively coupled LC resonant circuit shown in Fig 2.12(a).

Fig 2.12(b) shows it's equivalent circuit, where f_{op} and f_{sh} are the resonance frequencies when the symmetric plane $T(T')$ is open circuited (PMC) and short circuited (PEC), respectively. From the Fig 2.12(a) and (b), we have
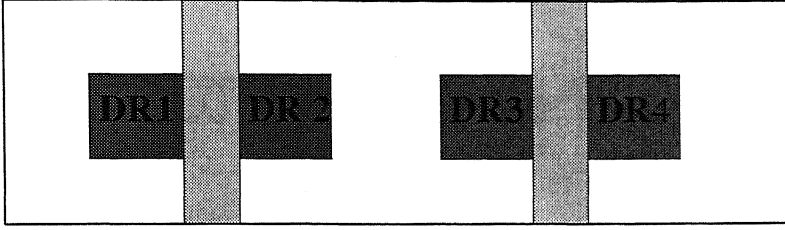
(a)
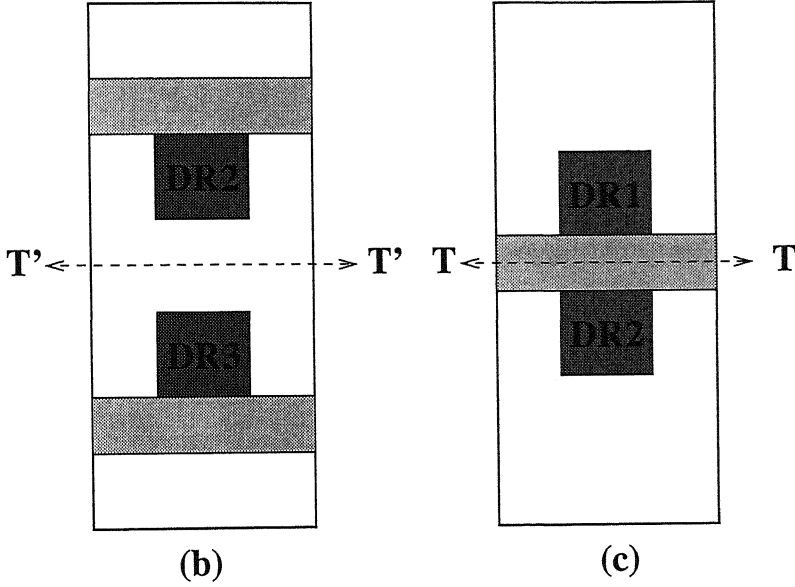
(b)　　　**(c)**

Figure 2.11: (a) Circuit configuration for inter-resonator coupling. (b) DRs having air in-between. (c) DRs having substrate in-between

$$f_0 = \frac{1}{2\pi\sqrt{LC}} \tag{2.34}$$

where f_0 is the resonance frequency of the LC resonant circuit (from Fig 2.12(a)).

$$f_{op} = f_0 \tag{2.35}$$

25
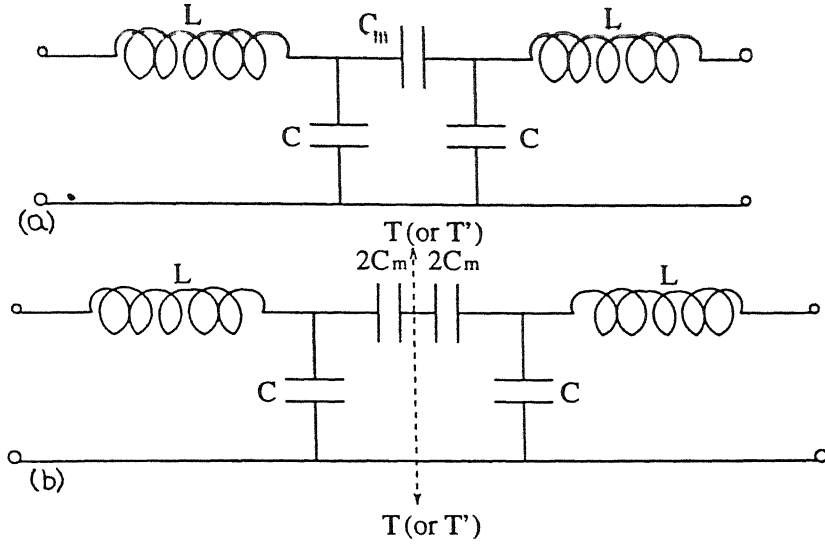
Figure 2.12: (a) Capacitively coupled LC resonant circuit. (b) Equivalent circuit.

$$f_{sh} = f_0 \left(\frac{1-k}{1+k} \right)^{1/2} \qquad (2.36)$$

where k is the inter-resonator coupling coefficient and is defined as [16]

$$k = \frac{C_m}{C + C_m} \qquad (2.37)$$

From equations (2.35) and (2.36), it can be shown that

$$k = \frac{f_{op}^2 - f_{sh}^2}{f_{op}^2 + f_{sh}^2} \qquad (2.38)$$

2.6.1   Numerical Implementation

f_{op} and f_{sh} can be found for both the structures shown in Fig 2.11(b) & (c), and therefore the inter-resonator coupling coefficient can be computed using equation (2.38). Fig 2.13 shows the comparison of computed results as against published data [16] for the structure of Fig 2.11(b) without any

26

substrate (i.e. $\epsilon_s = 1.0$), and neglecting the effect of dielectric support ($\epsilon_s = 1.03$) used in [16]. Here it can be observed that the present theory gives

$h_1 = h_2$=3mm, ϵ_d=24, ϵ_s=5, d=3.635mm, a=5.45mm,

2h=4.04mm
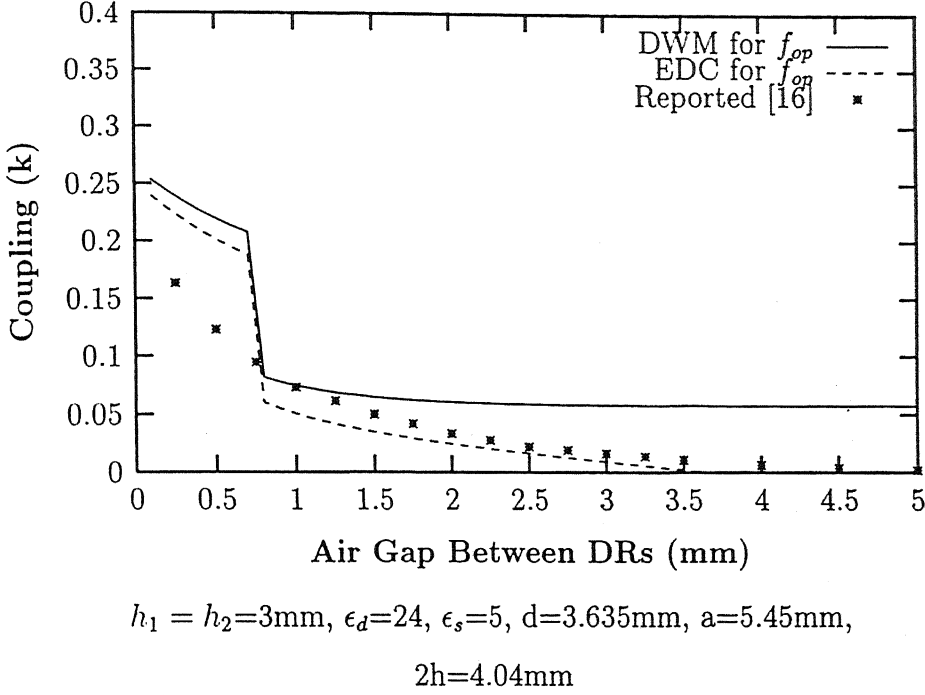
Figure 2.13: Comparison of computed inter-resonator coupling with published data in [16].

slightly higher results for inter-resonator coupling coefficient for very small air gap and very low results thereafter, which is due to the slight error in the computation of f_{op} (being slightly high by pure DWM method) and f_{sh} (being slightly low by the modified DWM method). However, the result achieved is that, the inter-resonator coupling reduces rapidly as the distance between the two dielectric resonators increases, and that they couple electrically with each other when the dominant evanescent waveguide mode is the TM mode.

Chapter 3

Energy Distribution

The relative energy distribution in different regions of the circuit structure involving dielectric resonator, is very useful in deciding how to do the coupling of DR with the other components. This chapter will deal with the electric and magnetic energy distribution for $TM_{01\delta}$ mode at resonance.

3.1 Electrical Energy Distribution

Total electrical energy stored in the structure given in Fig 2.1, is the sum of individual electrical energy stored in each region. It may be calculated from the field expressions derived in chapter 2.

$$W_e = \sum_{i=1}^{6} W_{ei} \tag{3.1}$$

where, W_{ei} is the electrical energy stored in the i_{th} region of the structure occupying volume V and having dielectric constant ϵ_{ri}. W_{ei} is given by :-

$$W_{ei} = \frac{\epsilon_0 \epsilon_{ri}}{4} \int_V \vec{E_i} \cdot \vec{E_i^*} \, dv \tag{3.2}$$

Where, '*' indicates the complex conjugate. For $TM_{01\delta}$ mode only E_z and E_r components of electric field exist, therefore for different regions we get stored electrical energy as follows :-

Region 1

$$W_{e1} = \frac{\epsilon_0 \epsilon_d}{4} \int_0^d \int_0^{2\pi} \int_{-h}^h \left(\vec{E}_{z1} \cdot \vec{E}_{z1}^* + \vec{E}_{r1} \cdot \vec{E}_{r1}^* \right) r \, dr \, d\phi \, dz \qquad (3.3)$$

Region 2

$$W_{e2} = \frac{\epsilon_0}{4} \int_0^d \int_0^{2\pi} \int_h^{h_4} \left(\vec{E}_{z2} \cdot \vec{E}_{z2}^* + \vec{E}_{r2} \cdot \vec{E}_{r2}^* \right) r \, dr \, d\phi \, dz \qquad (3.4)$$

Region 3

$$W_{e3} = \frac{\epsilon_0 \epsilon_s}{4} \int_0^d \int_0^{2\pi} \int_{-h_3}^{-h} \left(\vec{E}_{z3} \cdot \vec{E}_{z3}^* + \vec{E}_{r3} \cdot \vec{E}_{r3}^* \right) r \, dr \, d\phi \, dz \qquad (3.5)$$

Region 4

$$W_{e4} = \frac{\epsilon_0}{4} \int_d^a \int_0^{2\pi} \int_h^{h_4} \left(\vec{E}_{z4} \cdot \vec{E}_{z4}^* + \vec{E}_{r4} \cdot \vec{E}_{r4}^* \right) r \, dr \, d\phi \, dz \qquad (3.6)$$

Region 5

$$W_{e5} = \frac{\epsilon_0}{4} \int_d^a \int_0^{2\pi} \int_{-h}^h \left(\vec{E}_{z5} \cdot \vec{E}_{z5}^* + \vec{E}_{r5} \cdot \vec{E}_{r5}^* \right) r \, dr \, d\phi \, dz \qquad (3.7)$$

Region 6

$$W_{e6} = \frac{\epsilon_0 \epsilon_s}{4} \int_d^a \int_0^{2\pi} \int_{-h_3}^{-h} \left(\vec{E}_{z6} \cdot \vec{E}_{z6}^* + \vec{E}_{r6} \cdot \vec{E}_{r6}^* \right) r \, dr \, d\phi \, dz \qquad (3.8)$$

After substituting the values of fields from chapter 2, and solving integrals, we get the expressions for these electrical energies as follows :-

Note :- Here the upper term in square bracket [ ] corresponds to corresponding circular plate of cavity to be PEC and lower term corresponds to the

corresponding plate of the cavity to be PMC.

$$W_{e1} = A_0\epsilon_d \left\{ A_{16}\, I_{J0} + \beta_1^2\, A_{16}'\, A_{1234} \right\} \tag{3.9}$$

$$W_{e2} = A_0 B_2^2 \left\{ \begin{bmatrix} t'_{(h_2,h_4,\alpha_a)} \\ t_{(h_2,h_4,\alpha_a)} \end{bmatrix} I_{J0} + \alpha_a^2 \begin{bmatrix} t_{(h_2,h_4,\alpha_a)} \\ t'_{(h_2,h_4,\alpha_a)} \end{bmatrix} A_{1234} \right\} \tag{3.10}$$

$$W_{e3} = A_0 B_3^2 \epsilon_s \left\{ \begin{bmatrix} t'_{(h_1,h_3,\alpha_s)} \\ t_{(h_1,h_3,\alpha_s)} \end{bmatrix} I_{J0} + \alpha_s^2 \begin{bmatrix} t_{(h_1,h_3,\alpha_s)} \\ t'_{(h_1,h_3,\alpha_s)} \end{bmatrix} A_{1234} \right\} \tag{3.11}$$

$$W_{e4} = A_0 B_5^2 \left\{ \begin{bmatrix} t'_{(h_2,h_4,\alpha_a)} \\ t_{(h_2,h_4,\alpha_a)} \end{bmatrix} I_{KI0} + \alpha_a^2 \begin{bmatrix} t_{(h_2,h_4,\alpha_a)} \\ t'_{(h_2,h_4,\alpha_a)} \end{bmatrix} A_{5678} \right\} \tag{3.12}$$

$$W_{e5} = A_0 B_6^2 \left\{ A_{16}\, I_{KI0} + \beta_1^2\, A_{16}'\, A_{5678} \right\} \tag{3.13}$$

$$W_{e6} = A_0 B_7^2 \epsilon_s \left\{ \begin{bmatrix} t'_{(h_1,h_3,\alpha_s)} \\ t_{(h_1,h_3,\alpha_s)} \end{bmatrix} I_{KI0} + \alpha_s^2 \begin{bmatrix} t_{(h_1,h_3,\alpha_s)} \\ t'_{(h_1,h_3,\alpha_s)} \end{bmatrix} A_{5678} \right\} \tag{3.14}$$

where,

$$A_0 = \frac{\epsilon_0 \pi}{2} \tag{3.15}$$

$$A_{1234} = \frac{I_{EJ}}{k_r^2} \tag{3.16}$$

$$A_{5678} = \frac{I_{EKI}}{k_a^2} \tag{3.17}$$

Here constants B_{is} are same as in chapter 2, and are given at Appendix A. Other constants are given at Appendix B.

3.1.1   Electric Energy Filling Factor

Energy filling factor is an important quantity used in connection with the analysis of partially filled cavities. This is defined as the ratio of the electric energy for a given region to the total electric energy stored in the system. Based on the above analysis for electric energy, a program has been developed to find the energy in all the regions of the structure. Results obtained are tabulated in terms of energy filling factor for each region for different dielectric constants of the resonator and the substrate. It can be observed from the Table 3.1, that for $\epsilon_d = 38.0$, more electrical energy gets confined

Table 3.1: Electric energy filling factor for various regions of resonant structure

$d = 3.635mm, \quad a = 5.45mm, \quad h_1 = 2.0mm, \quad h_2 = 2.0mm, \quad 2h = 4.04mm$

ϵ_d	ϵ_s	Energy Filling Factor ($= W_{ei}/W_e$)% for region No.					
		1	2	3	4	5	6
24.0	2.22	51.96	0.476	1.156	6.618	24.58	15.20
30.0	2.22	54.50	0.383	0.914	6.225	23.76	14.20
30.0	10.0	34.12	0.209	3.933	3.870	13.45	44.40
38.0	2.22	56.79	0.305	0.715	5.879	22.96	13.34

within the resonator than when ϵ_d=24.0, therefore energy leakage in other regions increases when dielectric constant of DR (ϵ_d) decreases. Similarly, using higher dielectric constant substrate, energy contents in the region 3 and 6 increases. Also, since about 40-50% electrical energy is distributed in outer regions, electric coupling of the DR (in $TM_{01\delta}$ mode); with other circuit elements is very strong.

3.2   Magnetic Energy Distribution

We can also find the magnetic energy stored in the structure in Fig 2.1, in the same way as we have done for the electric energy. The net magnetic energy is the sum of magnetic energies of individual regions.

$$W_m = \sum_{i=1}^{6} W_{mi} \tag{3.18}$$

where, W_{mi} is the magnetic energy stored in the i_{th} region of the structure occupying volume V and having relative permeability μ_{ri}. W_{mi} is given by :-

$$W_{mi} = \frac{\mu_0 \mu_{ri}}{4} \int_V \vec{H}_i \cdot \vec{H}_i^* \, dv \tag{3.19}$$

31

For $TM_{01\delta}$ mode only H_ϕ component of magnetic field exists, therefore for different regions we get stored magnetic energy as follows :-

Region 1

$$W_{m1} = \frac{\mu_0}{4} \int_0^d \int_0^{2\pi} \int_{-h}^h \left(\vec{H}_{\phi1} \cdot \vec{H}_{\phi1}^* \right) r \, dr \, d\phi \, dz \qquad (3.20)$$

Region 2

$$W_{m2} = \frac{\mu_0}{4} \int_0^d \int_0^{2\pi} \int_h^{h_4} \left(\vec{H}_{\phi2} \cdot \vec{H}_{\phi2}^* \right) r \, dr \, d\phi \, dz \qquad (3.21)$$

Region 3

$$W_{m3} = \frac{\mu_0}{4} \int_0^d \int_0^{2\pi} \int_{-h_3}^{-h} \left(\vec{H}_{\phi3} \cdot \vec{H}_{\phi3}^* \right) r \, dr \, d\phi \, dz \qquad (3.22)$$

Region 4

$$W_{m4} = \frac{\mu_0}{4} \int_d^a \int_0^{2\pi} \int_h^{h_4} \left(\vec{H}_{\phi4} \cdot \vec{H}_{\phi4}^* \right) r \, dr \, d\phi \, dz \qquad (3.23)$$

Region 5

$$W_{m5} = \frac{\mu_0}{4} \int_d^a \int_0^{2\pi} \int_{-h}^h \left(\vec{H}_{\phi5} \cdot \vec{H}_{\phi5}^* \right) r \, dr \, d\phi \, dz \qquad (3.24)$$

Region 6

$$W_{m6} = \frac{\mu_0}{4} \int_d^a \int_0^{2\pi} \int_{-h_3}^{-h} \left(\vec{H}_{\phi6} \cdot \vec{H}_{\phi6}^* \right) r \, dr \, d\phi \, dz \qquad (3.25)$$

After substituting the values of fields from chapter 2, and solving integrals, we get the expressions for these magnetic energies as follows :-

Note :- Here the upper term in square bracket [ ] corresponds to corresponding circular plate of cavity to be PEC and lower term corresponds to the

corresponding plate of the cavity to be PMC.

$$W_{m1} = D_0 \epsilon_d^2 \left\{ A_{16} A_{1234} \right\} \tag{3.26}$$

$$W_{m2} = D_0 B_2^2 \left[\begin{array}{c} t'_{(h_2,h_4,\alpha_a)} \\ t_{(h_2,h_4,\alpha_a)} \end{array} \right] A_{1234} \tag{3.27}$$

$$W_{m3} = D_0 B_3^2 \epsilon_s^2 \left[\begin{array}{c} t'_{(h_1,h_3,\alpha_s)} \\ t_{(h_1,h_3,\alpha_s)} \end{array} \right] A_{1234} \tag{3.28}$$

$$W_{m4} = D_0 B_5^2 \left[\begin{array}{c} t'_{(h_2,h_4,\alpha_a)} \\ t_{(h_2,h_4,\alpha_a)} \end{array} \right] A_{5678} \tag{3.29}$$

$$W_{m5} = D_0 B_6^2 \left\{ A_{16} A_{5678} \right\} \tag{3.30}$$

$$W_{m6} = D_0 B_7^2 \epsilon_s^2 \left[\begin{array}{c} t'_{(h_1,h_3,\alpha_s)} \\ t_{(h_1,h_3,\alpha_s)} \end{array} \right] A_{5678} \tag{3.31}$$

where,

$$D_0 = \frac{\mu_0 \pi \left(\omega_0 \epsilon_0 \right)^2}{2} \tag{3.32}$$

$$A_{1234} = \frac{I_{EJ}}{k_r^2} \tag{3.33}$$

$$A_{5678} = \frac{I_{EKI}}{k_a^2} \tag{3.34}$$

Here constants B_{is} are same as in chapter 2, and are given at Appendix A. Other constants are given at Appendix B.

3.2.1   Magnetic Energy Filling Factor

This factor for a region represents the part of total magnetic energy in that region. For $TM_{01\delta}$ mode, though it is not of much importance because most of the magnetic energy is contained within the dielectric resonator and almost negligible amount is in the other regions, therefore magnetic coupling is extremely weak for $TM_{01\delta}$ mode. Table 3.2 shows the magnetic energy distribution in all the regions of the structure. We can observe from Table 3.2 that as was expected most of the magnetic energy (90-95%) is stored within the DR and only fractional amount (5%) is distributed in the other regions.

Table 3.2: Magnetic energy filling factor for various regions of resonant structure

$d = 3.635mm, \quad a = 5.45mm, \quad h_1 = 3.0mm, \quad h_2 = 3.0mm, \quad 2h = 4.04mm$

ϵ_d	ϵ_s	Energy Filling Factor $(= W_{mi}/W_m)\%$ for region No.					
		1	2	3	4	5	6
24.0	2.22	91.12	0.029	0.166	0.791	4.289	3.605
30.0	2.22	93.354	0.018	0.100	0.576	3.283	2.667
30.0	10.0	70.793	0.010	2.780	0.378	2.840	23.19
38.0	2.22	95.070	0.011	0.059	0.417	2.482	1.957

As the dielectric constant of the DR increases the stored energy within the DR increases. therefore, magnetic energy does not play important role in the coupling, when operating in the $TM_{01\delta}$ mode.

Chapter 4

Unloaded Quality Factor (Q_0)

4.1 Quality Factor

Quality factor of a circuit is a very important parameter because it limits the overall performance of the circuit. Higher value of Q is required in design of narrowband filters. The unloaded Quality factor of a DR placed in an MIC environment or a PEC cavity, depends upon losses in the DR's material, conductor loss in the shielding walls and dielectric loss in the substrate. Many rigorous analysis methods have been reported to find the Q-factor which are quite accurate, but are highly complicated and numerical extensive. Frequency perterbation technique has been reported for computing the Q-factor for $TE_{01\delta}$ mode by Kajfez [17]. A similar approach can however be derived for computng the Q-factor for $TM_{01\delta}$ mode, for finding Q-factors due to dielectric rod (DR) loss, dielectric support loss, but it cannot be used for finding the Q-factor due to conductor losses [16]. Although this method is quite accurate, lot of caution may be required while applying this method, because the relative change in resonance frequency due to slight perterbation, is very large for close PEC walls and causes error.

In this thesis Q-factor is determined for the structure of Fig 2.1 by

computing the stored energy and power loss. This method is approximate but, is quite accurate and data calculated by this method can be used for design purposes.

4.1.1 Definition of Q-factor

The Q-factor is assurance of the performance or quality of resonator, and is a measure of energy loss or dissipation loss per cycle as compared to the stored energy. Q-factor is defined by the well known relation :-

$$Q \; = \; 2\,\pi \; \frac{max\ energy\ stored}{avg.\ energy\ dissipated\ per\ cycle} \tag{4.1}$$

Let W_e and W_m are the stored electric and magnetic energies respectively, f_0 is the resonance frequency and P is the total loss, then Q will be given by :-

$$Q \; = \; 2\,\pi \; \frac{(W_e \; + \; W_m)}{P/f_0} \tag{4.2}$$

4.2 Determination of Conductor Losses

The tangential magnetic field generates the conductor current on the top and bottom metal plates and cylindrical side plates of the waveguide section. Let $\vec{J_c}$ is the surface current density on the metal surfaces, then the conductor loss P_c can be expressed as :-

$$P_c \; = \; \frac{1}{2}\,R_s \; \int |\,\vec{J_c}\,|^2 \; ds \tag{4.3}$$

where, R_s is the real part of surface impedance and is given by :-

$$R_s \; = \; \sqrt{\pi\,f_0\,\mu_0\,/\,\sigma} \tag{4.4}$$

where, σ is the conductivity of the metal surfaces, and $\vec{J_c} = \hat{z} \times \vec{H}$, and $\hat{z}$ is the normal vector to the surface.

4.2.1   Losses in Top Circular Plate

The conductor losses in the top circular plate of the cavity can be given as :-

$$P_{c(top)} = \frac{1}{2} R_s \int |\vec{J}_{c(top)}|^2 \, ds$$

In $TM_{01\delta}$ mode only H_ϕ component of the magnetic field exists, hence $\vec{J}_{c(top)} = \hat{z} \times \vec{H}_\phi$ (for region 2 & 4).

Region 2

$$\vec{J}_{c2(top)} = \hat{z} \times \vec{H}_{\phi 2} \tag{4.5}$$

$$P_{c2(top)} = \frac{1}{2} R_s \left(\frac{\omega \epsilon_0 B_2}{k_r} \right)^2 e^{-2\alpha_a h_4} \int_0^{2\pi} \int_0^d J_1^2 (k_r r) \; r \, dr \, d\phi$$

$$\Rightarrow \; P_{c2(top)} = \pi R_s \left(\omega \epsilon_0 B_2 \right)^2 e^{-2\alpha_a h_4} A_{1234} \tag{4.6}$$

Region 4

$$\vec{J}_{c4(top)} = \hat{z} \times \vec{H}_{\phi 4} \tag{4.7}$$

$$P_{c4(top)} = \frac{1}{2} R_s \left(\frac{\omega \epsilon_0 B_5}{k_a} \right)^2 e^{-2\alpha_a h_4} \int_0^{2\pi} \int_d^a \left[K_1 (k_a r) + B I_1 (k_a r) \right]^2 \; r \, dr \, d\phi$$

$$\Rightarrow \; P_{c4(top)} = \pi R_s \left(\omega \epsilon_0 B_5 \right)^2 e^{-2\alpha_a h_4} A_{5678} \tag{4.8}$$

4.2.2   Losses in Bottom Circular Plate

Region 3

$$P_{c3(bot)} = \frac{1}{2} R_s \left(\frac{\omega \epsilon_0 \epsilon_s B_3}{k_r} \right)^2 e^{-2\alpha_s h_3} \int_0^{2\pi} \int_0^d J_1^2 (k_r r) \; r \, dr \, d\phi$$

$$\Rightarrow \; P_{c3(bot)} = \pi R_s \left(\omega \epsilon_0 \epsilon_s B_3 \right)^2 e^{-2\alpha_s h_3} A_{1234} \tag{4.9}$$

Region 6

$$P_{c6(bot)} = \frac{1}{2} R_s \left(\frac{\omega \epsilon_0 \epsilon_s B_7}{k_a} \right)^2 e^{-2\alpha_s h_3} \int_0^{2\pi} \int_d^a [K_1 (k_a r) + B I_1 (k_a r)]^2 \; r \; dr \; d\phi$$

$$\Rightarrow \quad P_{c6(bot)} = \pi R_s \left(\omega \epsilon_0 \epsilon_s B_7 \right)^2 e^{-2\alpha_s h_3} A_{5678} \qquad (4.10)$$

4.2.3 Losses in Cylindrical Side Walls

The conductor losses in cylindrical side walls of the cavity, will be due to H_ϕ component of magnetic field in Region 4, 5 and 6, and $\vec{J}_{c(side)} = \hat{r} \times \vec{H}_\phi$.

Region 4

$$P_{c4(side)} = \frac{1}{2} R_s \left(\frac{\omega \epsilon_0 B_5}{k_a} \right)^2 e^{-2\alpha_a h_4} K I_{456} \int_0^a \int_h^{h_4} [\cosh \{ \alpha_a (z - h_4) \}]^2 \; dr \; dz$$

$$\Rightarrow \quad P_{c4(side)} = \pi \, a \, R_s \left(\frac{\omega \epsilon_0 B_5}{k_a} \right)^2 K I_{456} \; t'_{(h_2, h_4, \alpha_a)} \qquad (4.11)$$

Region 5

$$P_{c5(side)} = \frac{1}{2} R_s \left(\frac{\omega \epsilon_0 B_6}{k_a} \right)^2 K I_{456} \int_0^a \int_{-h}^h [\cos (\beta_1 z) + B_1 \sin (\beta_1 z)]^2 \; dr \; dz$$

$$\Rightarrow \quad P_{c5(side)} = \pi \, a \, R_s \left(\frac{\omega \epsilon_0 B_6}{k_a} \right)^2 K I_{456} \; A_{16} \qquad (4.12)$$

Region 6

$$P_{c6(side)} = \frac{1}{2} R_s \left(\frac{\omega \epsilon_0 \epsilon_s B_7}{k_a} \right)^2 e^{-2\alpha_s h_3} K I_{456} \int_0^a \int_{-h_3}^{-h} [\cosh \{ \alpha_s (z + h_3) \}]^2 \; dr \; dz$$

$$\Rightarrow \quad P_{c6(side)} = \pi \, a \, R_s \left(\frac{\omega \epsilon_0 \epsilon_s B_7}{k_a} \right)^2 K I_{456} \; t'_{(h_1, h_3, \alpha_s)} \qquad (4.13)$$

where,

$$KI_{456} = [K_1 (k_a a) + B I_1 (k_a a)]^2$$

$$B = K_0 (k_a a) / I_0 (k_a a)$$

B_{is} are given at Appendix A and other constants are given at Appendix B.

4.3 Conductor Quality Factor (Q_c)

If total conductor loss is given by P_c then :-

$$P_c = \left(P_{c2(top)} + P_{c4(top)}\right) + \left(P_{c3(bot)} + P_{c6(bot)}\right) + \left(P_{c4(side)} + P_{c5(side)} + P_{c6(side)}\right)$$

$$\Rightarrow P_c = P_{c(top)} + P_{c(bot)} + P_{c(side)} \tag{4.14}$$

where, $P_{c(top)}$, $P_{c(bot)}$, $P_{c(side)}$ are the total conductor losses in top, bottom and side walls respectively. Q-factor due to conductor losses (Q_c) can be defined as :-

$$Q_c = 2\pi f_0 \frac{(W_e + W_m)}{P_c} \tag{4.15}$$

therefore, from equation (4.14) we get,

$$\frac{P_c}{2\pi f_0 (W_e + W_m)} = \frac{P_{c(top)}}{2\pi f_0 (W_e + W_m)} + \frac{P_{c(bot)}}{2\pi f_0 (W_e + W_m)} + \frac{P_{c(side)}}{2\pi f_0 (W_e + W_m)}$$

$$\Rightarrow \frac{1}{Q_c} = \frac{1}{Q_{c(top)}} + \frac{1}{Q_{c(bot)}} + \frac{1}{Q_{c(side)}} \tag{4.16}$$

where, $Q_{c(top)}$, $Q_{c(bot)}$, $Q_{c(side)}$ are the Q-factors due to conductor losses in top, bottom and side walls respectively.

4.4 Dielectric Quality Factor (Q_d)

Intrinsic Q-factor of the DR (Q_{dr}) is dependant upon the loss tangent of the DR material. Q_d of DR in MIC environment or in a cavity, does not exactly equals $1/\tan\delta$. It also depends upon electric energy distribution inside and outside the resonator [18]. A similar argument is applicable to Q-factor due to dielectric loss in the substrate. By definition Q_d is given by :-

$$Q_d = \omega \frac{W}{P_d} \tag{4.17}$$

where, $W = W_e + W_m \approx 2W_e$, and $P_d = 2\omega W_d \tan\delta$. Here, W_d is the electrical energy stored in the dielectric region [18].

Hence, Q-factor due to dielectric loss in different regions are :-

Q-factor due to dielectric losses in the DR is

$$Q_{dr} = \frac{W_e}{W_{e1}\,\tan\delta_{dr}} \qquad (4.18)$$

Q-factor due to dielectric losses in the substrate (Region 3 and 6) is:-

$$Q_{ds} = \frac{W_e}{(W_{e3} + W_{e6})\,\tan\delta_{ds}} \qquad (4.19)$$

Here, $\tan\delta_{dr}$ and $\tan\delta_{ds}$ are the loss tangents of the resonator and substrate respectively. Total dielectric loss in all the regions, is equal to:-

$$P_{dt} = \dot{P}_{dr} + P_{ds}$$

$$\Rightarrow \quad P_{dt} = 2\omega W_{e1}\tan\delta_{dr} + 2\omega\left(W_{e3} + W_{e6}\right)\tan\delta_{ds}$$

$$\Rightarrow \quad \frac{P_{dt}}{2\omega W_e} = \frac{W_{e1}\tan\delta_{dr}}{W_e} + \frac{(W_{e3} + W_{e6})\tan\delta_{ds}}{W_e}$$

$$\Rightarrow \quad \frac{1}{Q_{dt}} = \frac{1}{Q_{dr}} + \frac{1}{Q_{ds}}$$

$$\Rightarrow \quad Q_{dt} = \frac{W_e}{W_{e1}\tan\delta_{dr} + (W_{e3} + W_{e6})\tan\delta_{ds}} \qquad (4.20)$$

4.5 Overall Unloaded Q-factor (Q_0)

Once the conductor Q-factor and the Q-factor due to dielectric losses are calculated, overall unloaded Q-factor can be calculated as :-

$$\frac{1}{Q_0} = \frac{1}{Q_c} + \frac{1}{Q_{dt}} \qquad (4.21)$$

Table 4.1: Comparison of Q_{dr}, Q_c, and Q_0 with published data [16]

$d = 3.635mm$, $a = 5.45mm$, $h_1 = h_2 = 14.54mm$, $2h = 4.04mm$

$\epsilon_s = 1.0$, $\epsilon_d = 24$, $\tan\delta_{dr} = 4 \times 10^{-5}$, $\sigma = 52.2 \times 10^6 S/m$

	Q_{dr}	Q_c	Q_0
Reported [16]	31,000.00	1,00,000.00	23,000.00
Present Theory	37,189.13	1,58,451.50	30,119.88

Note :- Here effect due to support dielectric ($\epsilon_r = 1.031$) in [16] has been neglected.

4.6 Numerical Implementation

Based on the above analysis, a program has been developed to determine the overall unloaded Q-factor of a DR in an MIC environment or kept in a PEC cavity. The results have been generated to obtain the conductor Q-factor (Q_c), dielectric Q-factor (Q_{dt}) and overall unloaded Q-factor (Q_0) and these have been compared with published data [16] in Table 4.1. Data for Q_0 have also been generated for DR in MIC environment, as a function of substrate thickness (h_1), with different parameters such as top plate distance (h_2), ϵ_d, ϵ_s etc. and they are shown from Fig 4.1 to 4.5.

Fig 4.1 shows the variation of Q_c with substrate thickness for different values of h_2. It can be seen that, as the conductor plates are taken away from the DR, the conductor Q-factor increases, which is due to the decrease in the conductor losses in those plates due to decaying magnetic field with distance. This effect on Q_c causes the increase in the overall unloaded Q-factor, which can be seen in Fig 4.2. Fig 4.3 shows the effect of substrate dielectric constant i.e. the Q_0 decreases with increase in the substrate dielectric constant due to increase in the dielectric losses in the substrate. Fig 4.4 shows the effect of DR dielectric constant over Q_0, and that also follows the same analogy of decrease in Q_0 with increase in the ϵ_d due to increase in the dielectric losses with increase in ϵ_d. Fig 4.5 shows that DR height also plays a role in
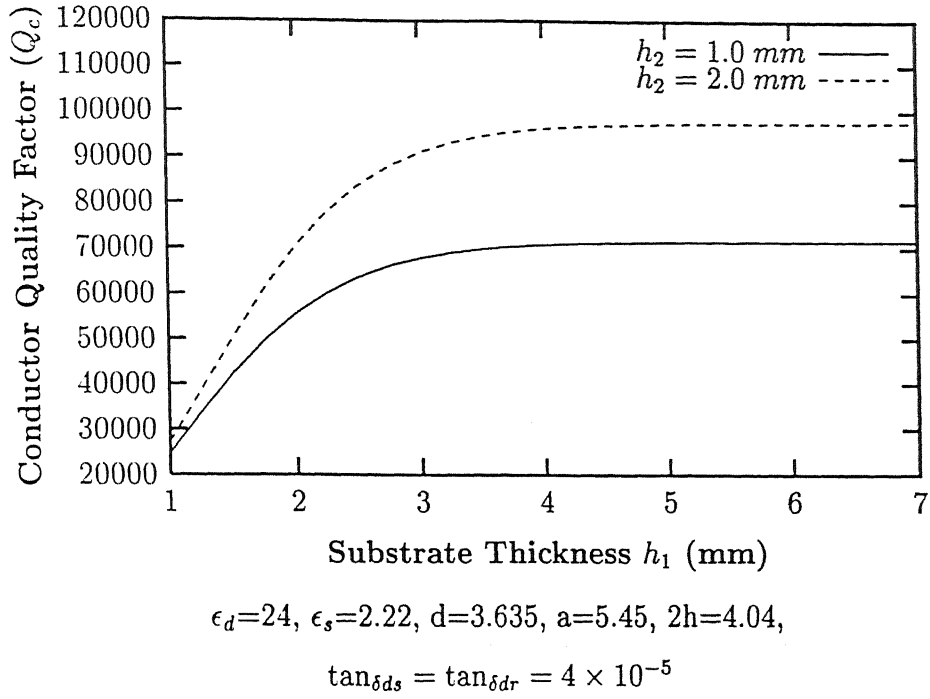
Figure 4.1: Variation of Q_c with conductor plate distance

$\epsilon_d=24$, $\epsilon_s=2.22$, d=3.635, a=5.45, 2h=4.04,

$$\tan_{\delta ds} = \tan_{\delta dr} = 4 \times 10^{-5}$$

controlling the Q_0, as with increase in DR height, the resonance frequency decreases and thereby decreasing the losses. Therefore Q_0 improves with the increase in the DR height.
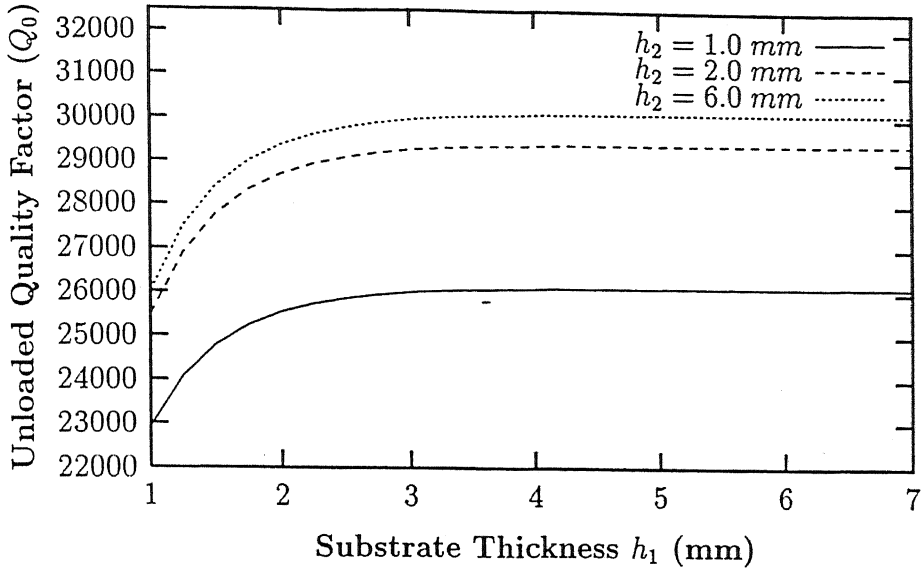
$\epsilon_d = 24$, ϵ_s=1, d=3.635, a=5.45, 2h=4.04, $\tan_{\delta dr} = 4 \times 10^{-5}$

Figure 4.2: Variation of Q_0 with conductor plate distance
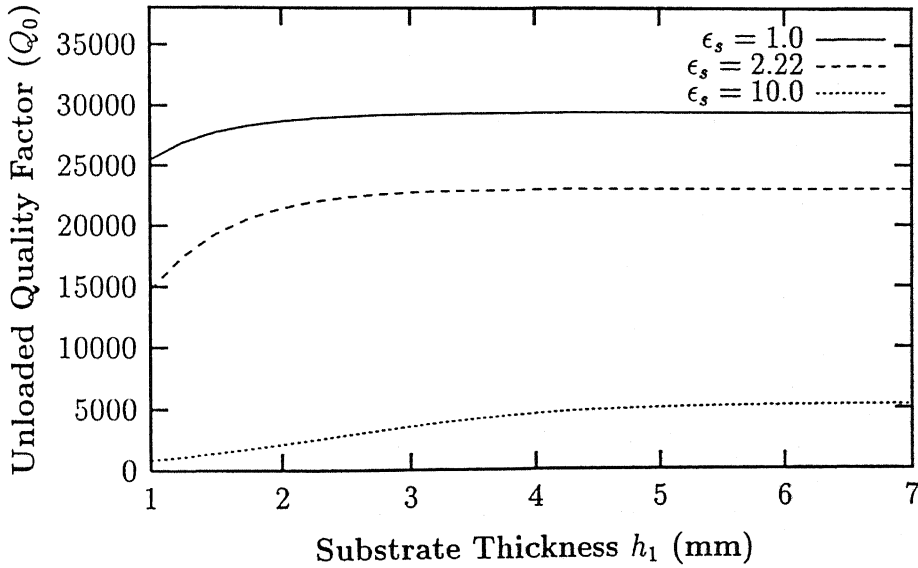
ϵ_d=24, h_2=2.0, d=3.635, a=5.45, 2h=4.04, $\tan_{\delta ds} = \tan_{\delta dr} = 4 \times 10^{-5}$

Figure 4.3: Variation of Q_0 with conductor plate distance, for different values of substrate dielectric constant (ϵ_s)
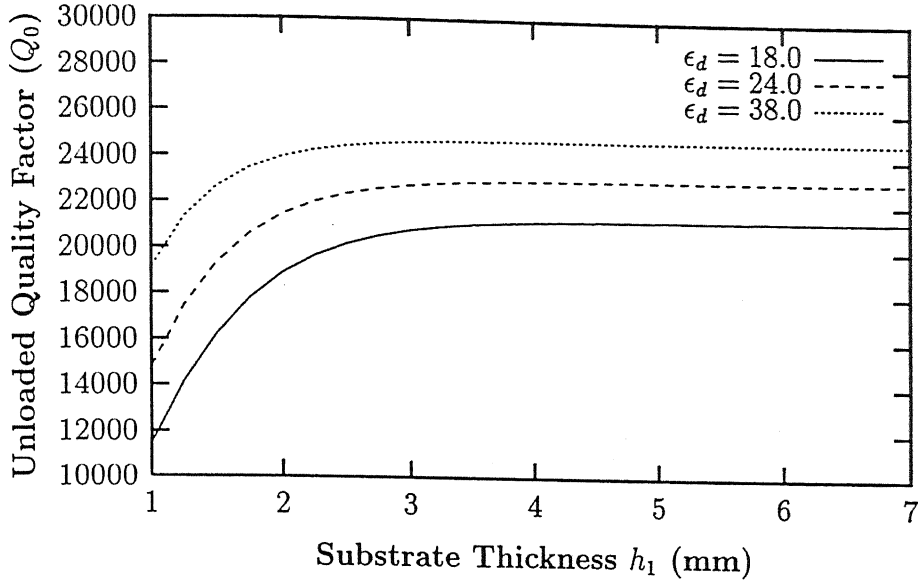
ϵ_s=2.22, h_2=2.0, d=3.635, a=5.45, 2h=4.04, $\tan_{\delta ds} = \tan_{\delta dr} = 4 \times 10^{-5}$

Figure 4.4: Variation of Q_0 with conductor plate distance, for different values of DR dielectric constant (ϵ_d)
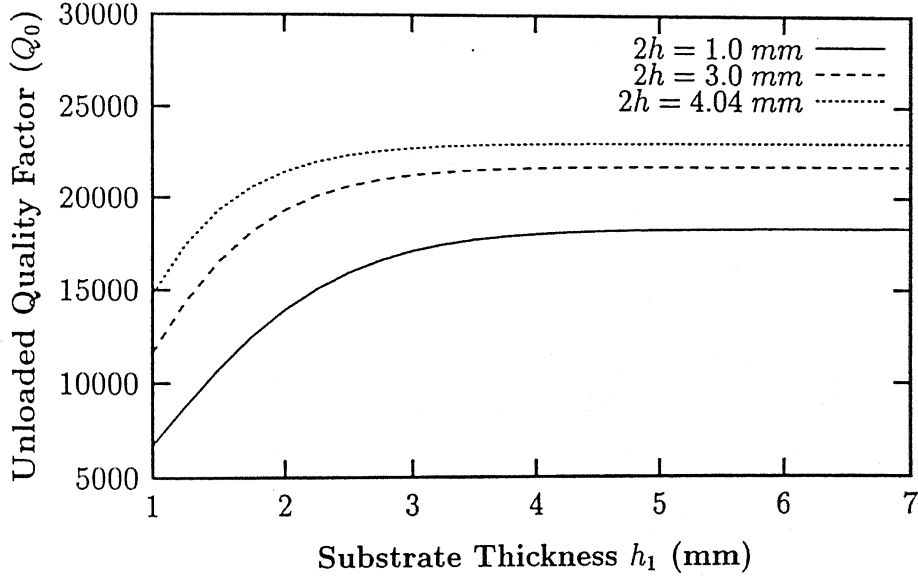
ϵ_s=2.22, ϵ_d=24.0, h_2=2.0, d=3.635, a=5.45, $\tan_{\delta ds} = \tan_{\delta dr} = 4 \times 10^{-5}$

Figure 4.5: Variation of Q_0 with conductor plate distance, for different values of DR Height ($2h$)

Chapter 5

DR in a Generalised Structure

Inter-resonator coupling between two DRs, found in chapter2, gives very high (for close PEC) and very low (for far PEC) results. The main reason for this error, was the inaccuracy in determination of f_{sh} (resonance frequency of DR in a PEC cavity) and thereby the error was incorporated in determination of inter-resonator coupling using Kobayashi's method [16] and equation (2.38). In order to determine the inter-resonator coupling for the structures shown in Fig 2.11 (b)&(c), using Skalicky's method [19] and that reported by Byzery [20], a much more generalised cavity structure containing an axially symmetrically placed DR (Fig 5.1) was concieved.

The other major advantage which was achieved simultaneously, was that the structure of Fig 5.1 could be used for determination of resonance frequency of dielectric resonator operating in $TM_{01\delta}$ mode, in practically all the possible types of environments like Isolated DR, DR post, DR in MIC or suspended substrate environments etc.

5.1 Resonance Frequency

The resonance frequency of the structure in Fig 5.1, is found using pure DWM method, by deriving the trancendental equations exactly on the similar lines as done in chapter 2, for a six region structure. For ease of analysis, the structure of Fig 5.1(a) can be devided into ten regions as shown in Fig 5.1(b).

5.1.1 Field Distributions

Proceeding on exactly similar lines of section 2.2.2, the field equations and corresponding separation equations in all the ten regions, can easily be written as :-

Region 1

$$E_{z1} = \{\cos(\beta_1 z) + B_1 \sin(\beta_1 z)\} \ J_0(k_r r)$$

$$E_{r1} = -\frac{\beta_1}{k_r} \{B_1 \cos(\beta_1 z) - \sin(\beta_1 z)\} \ J_1(k_r r)$$

$$H_{\phi 1} = \frac{j\omega\epsilon_0\epsilon_d}{k_r} \{\cos(\beta_1 z) + B_1 \sin(\beta_1 z)\} \ J_1(k_r r)$$

$$k_r^2 = \epsilon_d k_0^2 - \beta_1^2 \tag{5.1}$$

Region 2

$$E_{z2} = B_2 \{\cos(\beta_2 z) + B_3 \sin(\beta_2 z)\} \ J_0(k_r r)$$

$$E_{r2} = -\frac{\beta_2}{k_r}B_2 \{B_3 \cos(\beta_2 z) - \sin(\beta_2 z)\} \ J_1(k_r r)$$

$$H_{\phi 2} = \frac{j\omega\epsilon_0\epsilon_{s4}}{k_r}B_2 \{\cos(\beta_2 z) + B_3 \sin(\beta_2 z)\} \ J_1(k_r r)$$

$$k_r^2 = \epsilon_{s4} k_0^2 - \beta_2^2 \tag{5.2}$$

Region 3

$$E_{z3} = B_4 \left[\begin{array}{c} \cosh\{\alpha_{s3}(z - h_6)\} \\ -\sinh\{\alpha_{s3}(z - h_6)\} \end{array} \right] \ e^{-\alpha_{s3}h_6} \ J_0(k_r r)$$

Figure 5.1: (a) Cylindrical dielectric resonator in a partially filled cylindrical metal waveguide. (b) Cross-sectional view of one stage.

$$E_{r3} = \frac{\alpha_{s3}}{k_r} B_4 \begin{bmatrix} -\sinh\{\alpha_{s3}(z-h_6)\} \\ \cosh\{\alpha_{s3}(z-h_6)\} \end{bmatrix} e^{-\alpha_{s3}h_6} J_1(k_r r)$$

$$H_{\phi3} = \frac{j\omega\epsilon_0\epsilon_{s3}}{k_r} B_4 \begin{bmatrix} \cosh\{\alpha_{s3}(z-h_6)\} \\ -\sinh\{\alpha_{s3}(z-h_6)\} \end{bmatrix} e^{-\alpha_{s3}h_6} J_1(k_r r)$$

$$k_r^2 = \epsilon_{s3}k_0^2 + \alpha_{s3}^2 \qquad\qquad (5.3)$$

Region 4

$$E_{z4} = B_5 \{\cos(\beta_3 z) + B_6 \sin(\beta_3 z)\} J_0(k_r r)$$

$$E_{r4} = -\frac{\beta_3}{k_r} B_5 \{B_6 \cos(\beta_3 z) - \sin(\beta_3 z)\} J_1(k_r r)$$

$$H_{\phi4} = \frac{j\omega\epsilon_0\epsilon_{s1}}{k_r} B_5 \{\cos(\beta_3 z) + B_6 \sin(\beta_3 z)\} J_1(k_r r)$$

$$k_r^2 = \epsilon_{s1}k_0^2 - \beta_3^2 \qquad\qquad (5.4)$$

Region 5

$$E_{z5} = B_7 \begin{bmatrix} \cosh\{\alpha_{s2}(z+h_8)\} \\ \sinh\{\alpha_{s2}(z+h_8)\} \end{bmatrix} e^{-\alpha_{s2}h_8} J_0(k_r r)$$

$$E_{r5} = \frac{\alpha_{s2}}{k_r} B_7 \begin{bmatrix} -\sinh\{\alpha_{s2}(z+h_8)\} \\ -\cosh\{\alpha_{s2}(z+h_8)\} \end{bmatrix} e^{-\alpha_{s2}h_8} J_1(k_r r)$$

$$H_{\phi5} = \frac{j\omega\epsilon_0\epsilon_{s2}}{k_r} B_7 \begin{bmatrix} \cosh\{\alpha_{s2}(z+h_8)\} \\ \sinh\{\alpha_{s2}(z+h_8)\} \end{bmatrix} e^{-\alpha_{s2}h_8} J_1(k_r r)$$

$$k_r^2 = \epsilon_{s2}k_0^2 + \alpha_{s2}^2 \qquad\qquad (5.5)$$

Region 6

$$E_{z6} = B_8 \begin{bmatrix} \cosh\{\alpha_{s3}(z-h_6)\} \\ -\sinh\{\alpha_{s3}(z-h_6)\} \end{bmatrix} e^{-\alpha_{s3}h_6} \{K_0(k_a r) - BI_0(k_a r)\}$$

$$E_{r6} = \frac{\alpha_{s3}}{k_a} B_8 \begin{bmatrix} \sinh\{\alpha_{s3}(z-h_6)\} \\ -\cosh\{\alpha_{s3}(z-h_6)\} \end{bmatrix} e^{-\alpha_{s3}h_6} \{K_1(k_a r) + BI_1(k_a r)\}$$

$$H_{\phi6} = \frac{j\omega\epsilon_0\epsilon_{s3}}{k_a} B_8 \begin{bmatrix} -\cosh\{\alpha_{s3}(z-h_6)\} \\ \sinh\{\alpha_{s3}(z-h_6)\} \end{bmatrix} e^{-\alpha_{s3}h_6} \{K_1(k_a r) + BI_1(k_a r)\}$$
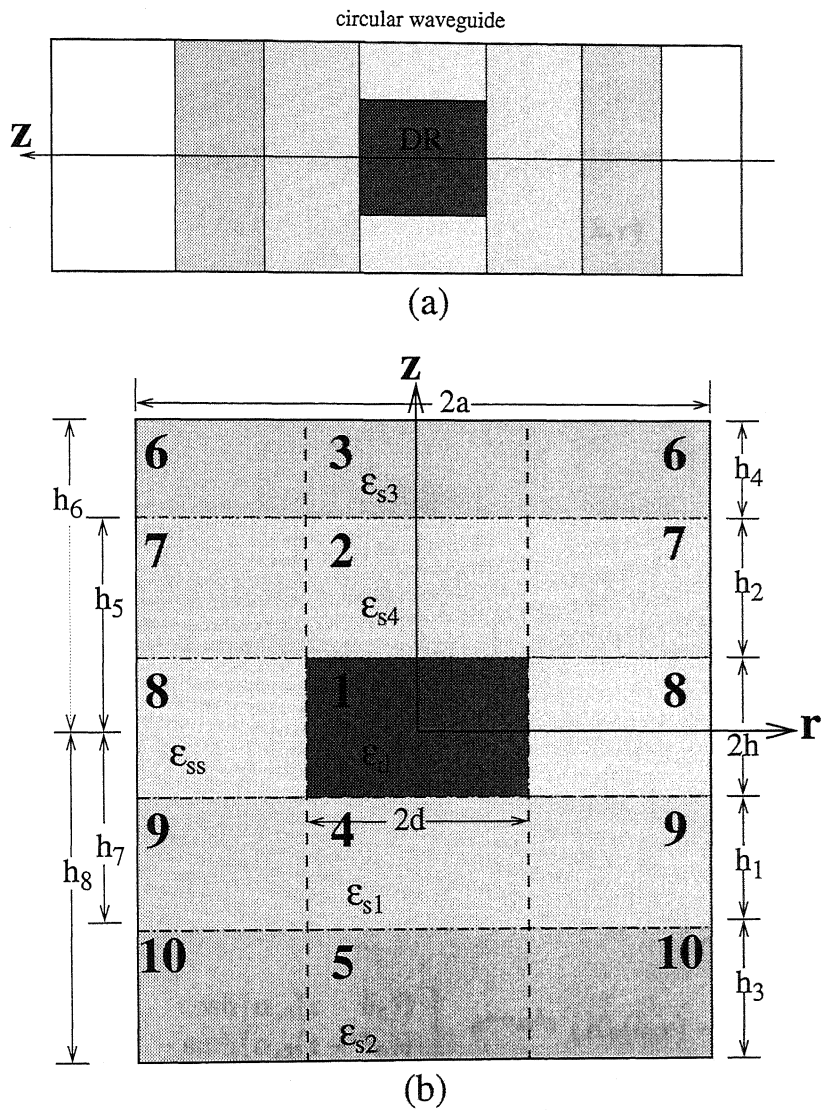
$$k_a^2 = -\epsilon_{s3}k_0^2 - \alpha_{s3}^2 \qquad\qquad (5.6)$$

Region 7

$$E_{z7} = B_9 \{\cos(\beta_2 z) + B_3 \sin(\beta_2 z)\} \{K_0(k_a r) - BI_0(k_a r)\}$$

$$E_{r7} = \frac{\beta_2}{k_a} B_9 \left\{ B_3 \cos(\beta_2 z) - \sin(\beta_2 z) \right\} \left\{ K_1(k_a r) + B I_1(k_a r) \right\}$$

$$H_{\phi 7} = -\frac{j\omega\epsilon_0\epsilon_{s4}}{k_a} B_9 \left\{ \cos(\beta_2 z) + B_3 \sin(\beta_2 z) \right\} \left\{ K_1(k_a r) + B I_1(k_a r) \right\}$$

$$k_a^2 = -\epsilon_{s4} k_0^2 + \beta_2^2 \tag{5.7}$$

Region 8

$$E_{z8} = B_{10} \left\{ \cos(\beta_1 z) + B_1 \sin(\beta_1 z) \right\} \left\{ K_0(k_a r) - B I_0(k_a r) \right\}$$

$$E_{r8} = \frac{\beta_1}{k_a} B_{10} \left\{ B_1 \cos(\beta_1 z) - \sin(\beta_1 z) \right\} \left\{ K_1(k_a r) + B I_1(k_a r) \right\}$$

$$H_{\phi 8} = -\frac{j\omega\epsilon_0\epsilon_{ss}}{k_a} B_{10} \left\{ \cos(\beta_1 z) + B_1 \sin(\beta_1 z) \right\} \left\{ K_1(k_a r) + B I_1(k_a r) \right\}$$

$$k_a^2 = -\epsilon_{ss} k_0^2 + \beta_1^2 \tag{5.8}$$

Region 9

$$E_{z9} = B_{11} \left\{ \cos(\beta_3 z) + B_6 \sin(\beta_3 z) \right\} \left\{ K_0(k_a r) - B I_0(k_a r) \right\}$$

$$E_{r9} = \frac{\beta_3}{k_a} B_{11} \left\{ B_6 \cos(\beta_3 z) - \sin(\beta_3 z) \right\} \left\{ K_1(k_a r) + B I_1(k_a r) \right\}$$

$$H_{\phi 9} = -\frac{j\omega\epsilon_0\epsilon_{s1}}{k_a} B_{11} \left\{ \cos(\beta_3 z) + B_6 \sin(\beta_3 z) \right\} \left\{ K_1(k_a r) + B I_1(k_a r) \right\}$$

$$k_a^2 = -\epsilon_{s1} k_0^2 + \beta_3^2 \tag{5.9}$$

Region 10

$$E_{z10} = B_{12} \begin{bmatrix} \cosh\{\alpha_{s2}(z + h_8)\} \\ \sinh\{\alpha_{s2}(z + h_8)\} \end{bmatrix} e^{-\alpha_{s2} h_8} \left\{ K_0(k_a r) - B I_0(k_a r) \right\}$$

$$E_{r10} = \frac{\alpha_{s2}}{k_a} B_{12} \begin{bmatrix} \sinh\{\alpha_{s2}(z + h_8)\} \\ \cosh\{\alpha_{s2}(z + h_8)\} \end{bmatrix} e^{-\alpha_{s2} h_8} \left\{ K_1(k_a r) + B I_1(k_a r) \right\}$$

$$H_{\phi 10} = -\frac{j\omega\epsilon_0\epsilon_{s2}}{k_a} B_{12} \begin{bmatrix} \cosh\{\alpha_{s2}(z + h_8)\} \\ \sinh\{\alpha_{s2}(z + h_8)\} \end{bmatrix} e^{-\alpha_{s2} h_8} \left\{ K_1(k_a r) + B I_1(k_a r) \right\}$$

$$k_a^2 = -\epsilon_{s2} k_0^2 - \alpha_{s2}^2 \tag{5.10}$$

Here,

$$B = K_0(k_a a) / I_0(k_a a) \tag{5.11}$$

Here also, upper term in the square brackets [ ] refers to the corresponding circular plate to be PEC and lower term refers to the corresponding circular plate to be PMC. Now, on applying the boundary conditions and equating the tangential field components at the boundary of each region and thereafter equating the expressions of like field constants, we get :-

$$\frac{J_0(k_r d)}{\{K_0(k_a d) - B I_0(k_a d)\}} + \frac{k_a \epsilon_d}{k_r \epsilon_{ss}} \frac{J_1(k_r d)}{\{K_1(k_a d) + B I_1(k_a d)\}} = 0 \qquad (5.12)$$

$$\frac{\epsilon_d \beta_2 + \epsilon_{s4} \beta_1 m_3 \tan(\beta_1 h)}{\epsilon_{s4} \beta_1 m_3 - \epsilon_d \beta_2 \tan(\beta_1 h)} - \frac{\epsilon_d \beta_3 - \epsilon_{s1} \beta_1 m_4 \tan(\beta_1 h)}{\epsilon_{s1} \beta_1 m_4 + \epsilon_d \beta_3 \tan(\beta_1 h)} = 0 \qquad (5.13)$$

where,

$$m_3 = \frac{1 + B_3 \tan(\beta_2 h)}{B_3 - \tan(\beta_2 h)} \qquad (5.14)$$

$$m_4 = \frac{1 - B_6 \tan(\beta_3 h)}{B_6 + \tan(\beta_3 h)} \qquad (5.15)$$

and,

$$\frac{\beta_2 \epsilon_{s3}}{\epsilon_{s4} \alpha_{s3}} \begin{bmatrix} \coth(\alpha_{s3} h_4) \\ \tanh(\alpha_{s3} h_4) \end{bmatrix} = \frac{1 + B_3 \tan(\beta_2 h_5)}{\tan(\beta_2 h_5) - B_3} = m_1 \ (say) \qquad (5.16)$$

$$\frac{\beta_3 \epsilon_{s2}}{\epsilon_{s1} \alpha_{s2}} \begin{bmatrix} \coth(\alpha_{s2} h_3) \\ \tanh(\alpha_{s2} h_3) \end{bmatrix} = \frac{1 - B_6 \tan(\beta_3 h_7)}{\tan(\beta_3 h_7) + B_6} = m_2 \ (say) \qquad (5.17)$$

Here, all the field constants (B_{is}) are given at Appendix C.

5.1.2 Numerical Implementation

Using the same approach of numerical implementation as used in chapter 2, we can find radial wave number (k_r) and axial wave number (β_1) and thereafter resonance frequency can be computed. A software package (DRTM10) has been developed for this implementation and all the results generated in chapter 2, have been again verified, thereby concluding the correctness of this analysis. Here also for top and bottom circular plates made of PEC, we have to use the modified DWM method as was done in section 2.3. Similar to equation (2.33) we get :-

$$\left(\frac{\epsilon_d \beta_2 + \epsilon_{s4} \beta_1 m_3 \tan(\beta_1 h)}{\epsilon_{s4} \beta_1 m_3 - \epsilon_d \beta_2 \tan(\beta_1 h)} - \frac{\epsilon_d \beta_3 - \epsilon_{s1} \beta_1 m_4 \tan(\beta_1 h)}{\epsilon_{s1} \beta_1 m_4 + \epsilon_d \beta_3 \tan(\beta_1 h)} \right) \cdot$$

$$\left(\frac{\epsilon_{ss} \beta_2 + \epsilon_{s4} \beta_1 m_3 \tan(\beta_1 h)}{\epsilon_{s4} \beta_1 m_3 - \epsilon_{ss} \beta_2 \tan(\beta_1 h)} - \frac{\epsilon_{ss} \beta_3 - \epsilon_{s1} \beta_1 m_4 \tan(\beta_1 h)}{\epsilon_{s1} \beta_1 m_4 + \epsilon_{ss} \beta_3 \tan(\beta_1 h)} \right) = 0 \quad (5.18)$$

5.1.3 Other Derived Structures

As it was mentioned earlier, using the structure of Fig 5.1, we can derive more structural environments for DR in $TM_{01\delta}$ mode, out of which isolated DR, DR post, DR in MIC environment and DR in a cylindrical cavity have already been discussed in chapter 2. The other structures are given in Fig 5.2 to Fig 5.3, for which the resonance frequency can be computed using same analysis and software package.

5.2 Energy Distribution

The electrical and magnetic energy distributions in each region of Fig 5.1, can be determined using the exactly same approach as done in chapter 3 for six regions structure of Fig 2.1. Therefore, here we will present only the final expressions for these energies.

$$\varepsilon_{S2} = \varepsilon_{SS} = \varepsilon_{S3} = \varepsilon_{S4} = 1.0$$

$a \longrightarrow \infty$ i.e. very large (say 5d)
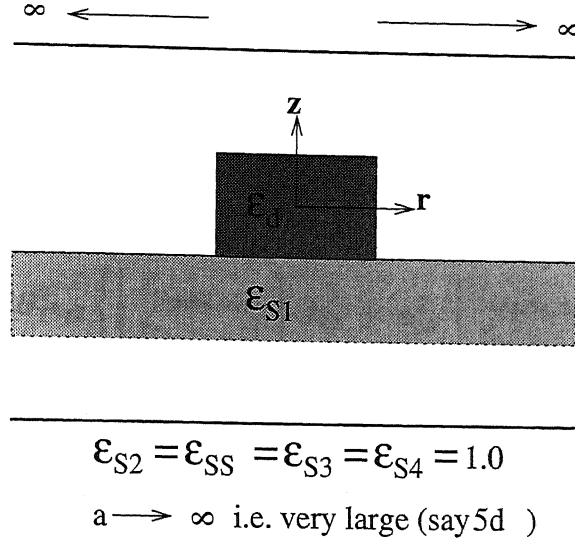
Figure 5.2: $TM_{01\delta}$ mode DR in suspended substrate MIC environment

$\varepsilon_{S1} = \varepsilon_{S2} = \varepsilon_{S3} = \varepsilon_{S4} = 1.0$
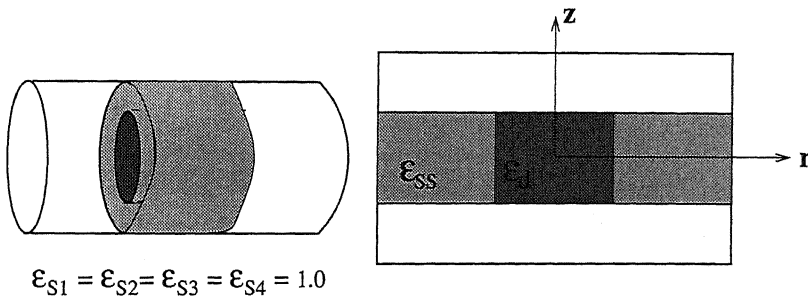
Figure 5.3: $TM_{01\delta}$ mode DR in a cylindrical (below cut-off) waveguide supported by a dielectric ring

5.2.1 Electrical Energy Distribution

The electrical energies in each region, are found to be as :-

$$W_{e1} = A_0\epsilon_d\left\{ A_{16} I_{J0} + \beta_1^2 A'_{16} A_{1234} \right\} \tag{5.19}$$

$$W_{e2} = A_0\epsilon_{s4}\left\{ A_{17} I_{J0} + A'_{17} A_{1234} \right\} \tag{5.20}$$

$$W_{e3} = A_0 B_4^2 \epsilon_{s3}\left\{ \begin{bmatrix} t'_{(h_4,h_6,\alpha_{s3})} \\ t_{(h_4,h_6,\alpha_{s3})} \end{bmatrix} I_{J0} + \alpha_{s3}^2 \begin{bmatrix} t_{(h_4,h_6,\alpha_{s3})} \\ t'_{(h_4,h_6,\alpha_{s3})} \end{bmatrix} A_{1234} \right\} \tag{5.21}$$

$$W_{e4} = A_0\epsilon_{s1}\left\{ A_{18} I_{J0} + A'_{18} A_{1234} \right\} \tag{5.22}$$

$$W_{e5} = A_0 B_7^2 \epsilon_{s2}\left\{ \begin{bmatrix} t'_{(h_3,h_8,\alpha_{s2})} \\ t_{(h_3,h_8,\alpha_{s2})} \end{bmatrix} I_{J0} + \alpha_{s2}^2 \begin{bmatrix} t_{(h_3,h_8,\alpha_{s2})} \\ t'_{(h_3,h_8,\alpha_{s2})} \end{bmatrix} A_{1234} \right\} \tag{5.23}$$

$$W_{e6} = A_0 B_8^2 \epsilon_{s3}\left\{ \begin{bmatrix} t'_{(h_4,h_6,\alpha_{s3})} \\ t_{(h_4,h_6,\alpha_{s3})} \end{bmatrix} I_{KI0} + \alpha_{s3}^2 \begin{bmatrix} t_{(h_4,h_6,\alpha_{s3})} \\ t'_{(h_4,h_6,\alpha_{s3})} \end{bmatrix} A_{5678} \right\} \tag{5.24}$$

$$W_{e7} = A_0 \frac{B_9^2}{B_2^2}\epsilon_{s4}\left\{ A_{17} I_{KI0} + A'_{17} A_{5678} \right\} \tag{5.25}$$

$$W_{e8} = A_0 B_{10}^2 \epsilon_{ss}\left\{ A_{16} I_{KI0} + \beta_1^2 A'_{16} A_{5678} \right\} \tag{5.26}$$

$$W_{e9} = A_0 \frac{B_{11}^2}{B_5^2}\epsilon_{s1}\left\{ A_{18} I_{KI0} + A'_{18} A_{5678} \right\} \tag{5.27}$$

$$W_{e10} = A_0 B_{12}^2 \epsilon_{s2}\left\{ \begin{bmatrix} t'_{(h_3,h_8,\alpha_{s2})} \\ t_{(h_3,h_8,\alpha_{s2})} \end{bmatrix} I_{KI0} + \alpha_{s2}^2 \begin{bmatrix} t_{(h_3,h_8,\alpha_{s2})} \\ t'_{(h_3,h_8,\alpha_{s2})} \end{bmatrix} A_{5678} \right\} \tag{5.28}$$

where,

$$A_0 = \frac{\epsilon_0 \pi}{2} \tag{5.29}$$

$$A_{1234} = \frac{I_{EJ}}{k_r^2} \tag{5.30}$$

$$A_{5678} = \frac{I_{EKI}}{k_a^2} \tag{5.31}$$

Here constants B_{is} are given at Appendix C and other constants are given at Appendix B.

5.2.2 Magnetic Energy Distribution

Similarly, the magnetic energy distribution in all the regions, is found to be as :-

$$W_{m1} = D_0 \epsilon_d^2 \{ A_{16} A_{1234} \} \tag{5.32}$$

$$W_{m2} = D_0 \epsilon_{s4}^2 \{ A_{17} A_{1234} \} \tag{5.33}$$

$$W_{m3} = D_0 \epsilon_{s3}^2 B_4^2 \begin{bmatrix} t'_{(h_4,h_6,\alpha_{s3})} \\ t_{(h_4,h_6,\alpha_{s3})} \end{bmatrix} A_{1234} \tag{5.34}$$

$$W_{m4} = D_0 \epsilon_{s1}^2 \{ A_{18} A_{1234} \} \tag{5.35}$$

$$W_{m5} = D_0 B_7^2 \epsilon_{s2}^2 \begin{bmatrix} t'_{(h_3,h_8,\alpha_{s2})} \\ t_{(h_3,h_8,\alpha_{s2})} \end{bmatrix} A_{1234} \tag{5.36}$$

$$W_{m6} = D_0 B_8^2 \epsilon_{s3}^2 \begin{bmatrix} t'_{(h_4,h_6,\alpha_{s3})} \\ t_{(h_4,h_6,\alpha_{s3})} \end{bmatrix} A_{5678} \tag{5.37}$$

$$W_{m7} = D_0 \frac{B_9^2}{B_2^2} \epsilon_{s4}^2 \{ A_{17} A_{5678} \} \tag{5.38}$$

$$W_{m8} = D_0 B_{10}^2 \epsilon_{ss}^2 \{ A_{16} A_{5678} \} \tag{5.39}$$

$$W_{m9} = D_0 \frac{B_{11}^2}{B_5^2} \epsilon_{s1}^2 \{ A_{18} A_{5678} \} \tag{5.40}$$

$$W_{m10} = D_0 B_{12}^2 \epsilon_{s2}^2 \begin{bmatrix} t'_{(h_3,h_8,\alpha_{s2})} \\ t_{(h_3,h_8,\alpha_{s2})} \end{bmatrix} A_{5678} \tag{5.41}$$

where,

$$D_0 = \frac{\mu_0 \pi (\omega_0 \epsilon_0)^2}{2} \tag{5.42}$$

$$A_{1234} = \frac{I_{EJ}}{k_r^2} \tag{5.43}$$

$$A_{5678} = \frac{I_{EKI}}{k_a^2} \tag{5.44}$$

5.2.3 Numerical Implementation

Using the electrical and magnetic energies formulated in previous sections, we can easily obtain the energy filling factors thereby finding the percentage energy in each region, as done in chapter 3. Also, the total electrical
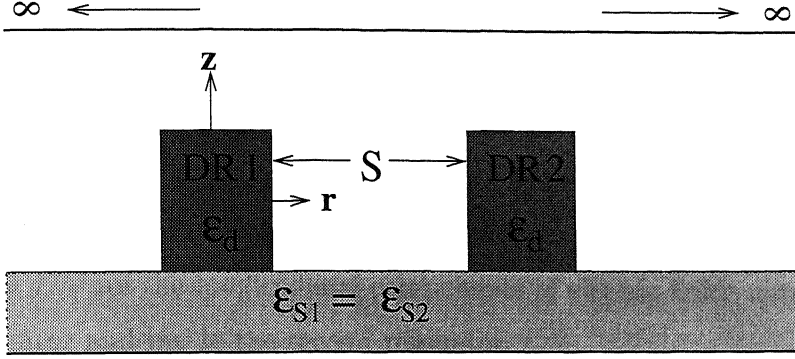
Figure 5.4: Edge coupled DRs placed in an MIC environment

and magnetic energies can be computed and used in determination of Q-factor, inter-resonator coupling etc.

5.3 Inter-Resonator Coupling

Using the versatality of the structure in Fig 5.1, it is possible to determine the coupling between two adjascent DRs, kept in environments like in Fig 2.11(b&c), which can be called as broad-side coupling and in Fig 5.4 which can be called as edge coupling. Skalicky [19] has reported the method for computation of inter-resonator coupling for $TE_{01\delta}$ mode using EM induction and reaction concept. He has assumed the DRs operating in $TE_{01\delta}$ mode to be acting as magnetic dipoles (i.e. current carrying loops) and thereby induction of voltage into adjacent second loop, due to the current in the first one, using the inductive coupling between the two DRs. A detailed analysis based on this method has been carried out in [6] for $TE_{01\delta}$ mode, for determination of both broad-side and edge coupling between two adjascent DRs. Byzery [20] has used the similar approach for fiding the edge coupling between the two adjascent DRs kept on a substrate, in rectangular waveguide (below cut-off) longitudanally, operating in $TM_{01\delta}$ mode. On the similar approach, a formulation has been done to find inter-resonator cou-

plings between adjascent DRs kept in environments of Fig 2.11(b&c) and Fig 5.4. The relation used in [20] based on [6] is given by :-

$$|k| = \frac{\epsilon_0 (\epsilon_r - 1)}{2 \, W_e} \int_V \vec{E}_{z1} \cdot \vec{E}_{z2} \, dv \qquad (5.45)$$

where k is the inter-resonator coupling, W_e is the total electrical energy stored and E_{z1} & E_{z2} are the longitudanal components of electric fields outside the first resonator and inside the second resonator.

5.3.1   Edge Coupled DRs

To find the inter-resonator edge-coupling between two adjascent DRs, shown in Fig 5.4 ($a \to \infty$ i.e. very large say $\approx 5d$), we need to find the volume integral in equation (5.45).

$$\int_V \vec{E}_{z1} \cdot \vec{E}_{z2} \, dv = \int_{-h}^{h} \int_0^{2\pi} \int_0^d E_{z8} E_{z1} \left\{ \frac{r + (2d + s) \sin \phi}{r'} \right\} r \, dr \, d\phi \, dz \qquad (5.46)$$

where,

$$r' = \left[r^2 + (2d + s)^2 + 2 (2d + s) \, r \sin \phi \right]^{1/2} \qquad (5.47)$$

Here, s is the edge-to-edge inter-resonator gap, as shown in Fig 5.4. Here E_{z1} will correspond to the E_z field in eight region of DR1 and E_{z2} will correspond to the E_z field in the first region (DR) of DR2. On substituting the values of E_{z8} and E_{z1} from section 5.1.1 into equation (5.46), the volume integral can be evaluated as :-

$$\int_V \vec{E}_{z1} \cdot \vec{E}_{z2} \, dv = B_{10} A_{16} I_{KO} \qquad (5.48)$$
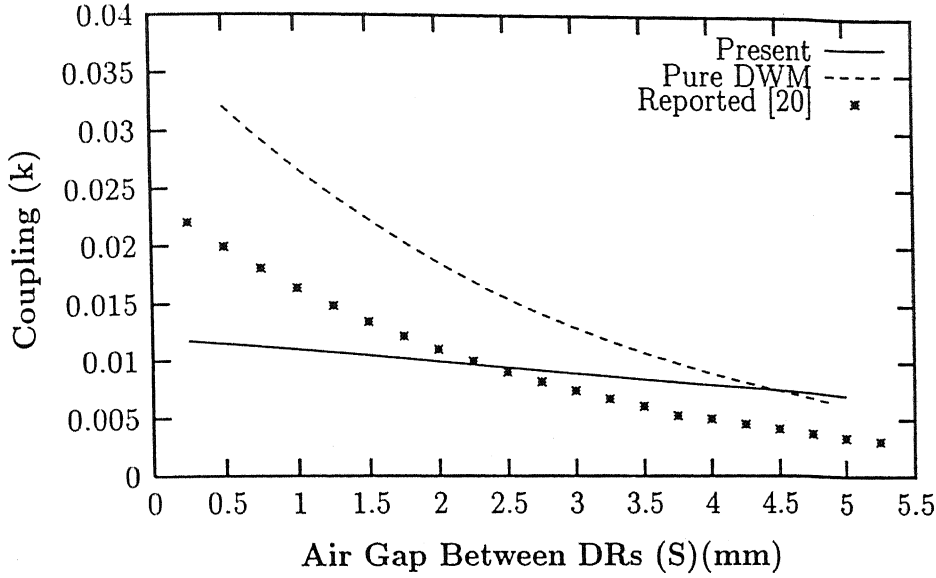
$h_1 = h_3 = 0.4$mm, $h_2 = h_4 = 1.575$mm, $\epsilon_{s1} = \epsilon_{s2} = 2.54$, $\epsilon_d = 24$, Th$=8.25$mm

Figure 5.5: Comparison of Inter-resonator edge-coupling with data published in [20]

5.3.3   Numerical Implimentation

A software package (DRTM10) has been developed for the entire analysis of the generalised structure of Fig 5.1. The results of inter-resonator coupling have been found to be very encouraging. Results of remaining parameters like resonance frequency, energy etc. are found to be the same as that in chapter2, and therefore those are not being shown here again.

Edge Coupling

The results for inter-resonator edge-coupling as a function of gap between the resonators, shown in Fig 5.4, have been plotted in Fig 5.5 which have also been compared with the results published in [20].

is as expected because as substrate dielectric constant increases, more electrical energy gets stored in the substrate region and therefore more interaction with other DR takes place. Also, it is seen that Pure DWM method gives higher results for higher substrate dielectric constant, than that calculated by Present method, however the nature of variation of coupling with substrate gap, is same in both the cases.

Fig 5.8 shows the variation in coupling between DRs through the air, as shown in Fig 2.11(b). This coupling has been calculated using both, Present method and the Pure DWM method. It is seen that this coupling however reduces with the increase in the substrate dielectric constant, because as the substrate dielectric constant increases more electrical energy gets attracted towards the substrate region and lesser energy gets stored in the air-gap region and therefore less interaction with the other DR takes place. Here also, the Pure DWM mehod gives higher results than that obtained from Present method, however the nature of coupling variation is same in both the cases.

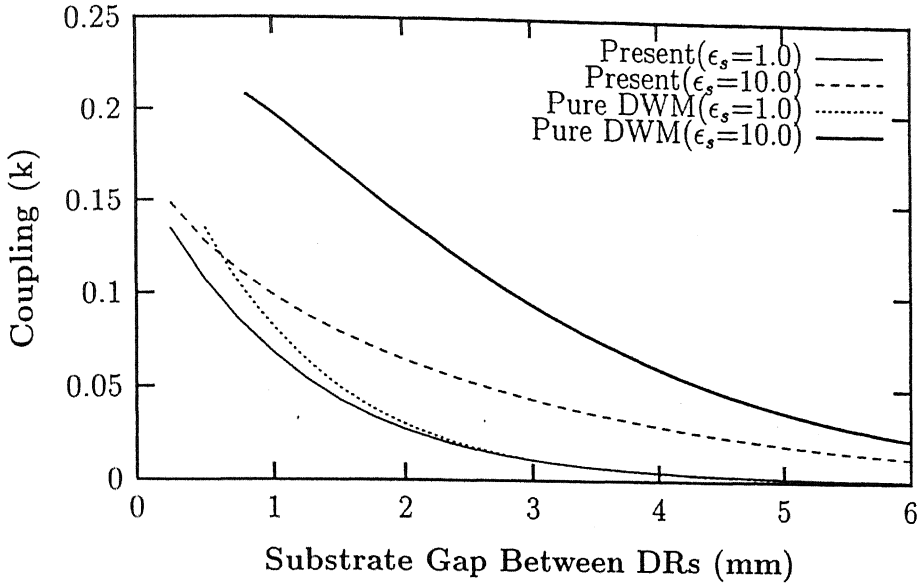Figure 5.7: Variation of Inter-resonator coupling with substrate thickness

h_2=1.0mm, $h_3 = h_4$=5.0mm, ϵ_d=24, d=3.635mm,

a=5.45mm, $\epsilon_{s2} = \epsilon_{s3} = \epsilon_{s4}$=1.0, Th=4.04mm
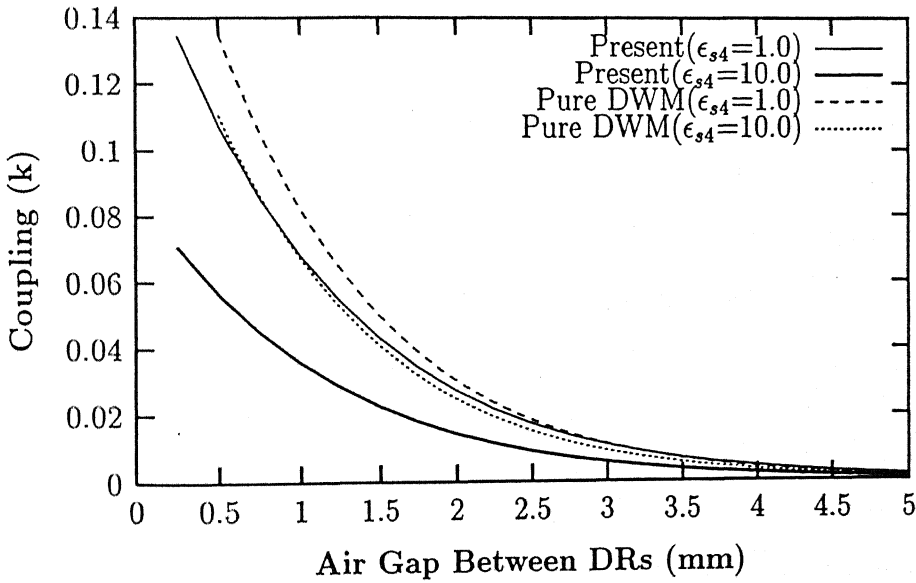
h_2=1.0mm, $h_3 = h_4$=5.0mm, ϵ_d=24, d=3.635mm,

a=5.45mm, $\epsilon_{s2} = \epsilon_{s3} = \epsilon_{s1}$=1.0, Th=4.04mm

Figure 5.8: Variation of Inter-resonator coupling with Air gap

Chapter 6

Filter Design

6.1 TM Mode DR Filter in Circular Waveguide Below Cut-off

Bandpass filters constructed by placing $TE_{01\delta}$ mode DRs co-axially in a TE_{01} mode cut-off circular cylindrical waveguide, have been reported [21]. For filters using the $TM_{01\delta}$ mode of DRs, on the other hand only few investigations have been presented [16], [20]. Filters using $TM_{01\delta}$ mode have been reported to have low loss operation [16] and a reduced excitation of spurious resonances as compared to $TE_{01\delta}$ mode filters [20]. In fact input and output couplings, realized by means of simple circular co-axial probes of suitable dimensions, allow excitation of only TM_{0n} modes in the circular waveguide, therefore avoiding spurious resonances of TE_{0n} modes as well as those of hybrid modes for the circular symmetry of the structure. However, the choice of $TM_{01\delta}$ resonance results in a longer structure than that obtained with the $TE_{01\delta}$ mode, for the same waveguide diameter.
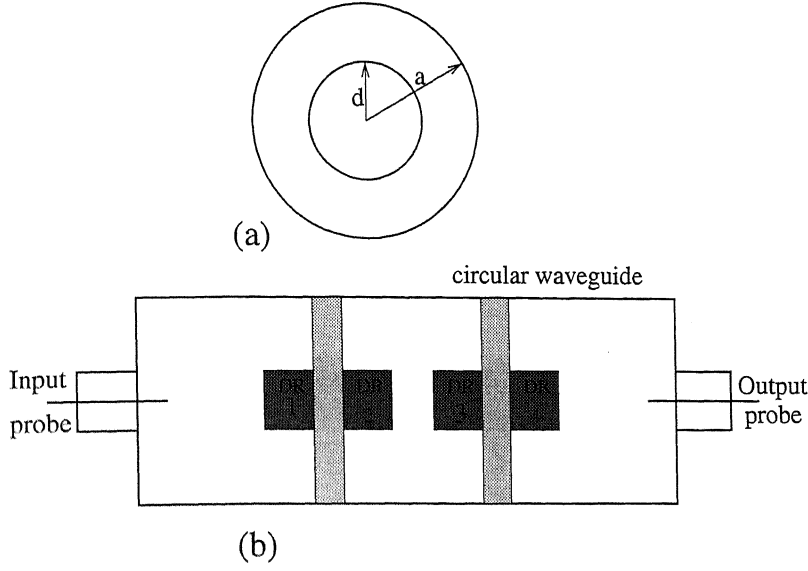
Figure 6.1: Filter Structure (a) Cross-sectional view (b) Longitudanal view.

6.2   Design Aspects

The filter structure having axially symmetric DR placed in a circular waveguide below cut-off will have a cross sectional view as shown in Fig 6.1. The excited TM mode in the structure must be above cut-off inside the dielectric loaded sections and below cut-off in the empty waveguide sections, thus the constraint on waveguide radius a is, that it must be smaller than a maximum value a_{max} given by :-

$$a_{max} = \frac{v_0}{2 \pi f_0} \chi \qquad (6.1)$$

where, v_0 is the velocity of light in the free space, f_0 is the filter bandpass center frequency and χ is the eigen value of the TM_{01} in the empty waveguide ($= 2.40482$).

6.2.1 Criterian for Selection of Parameters a and d

The relevant targets to be achieved by proper design are :-

1. Adequate limitation of the filter passband losses

2. Adequate reduction of spurious passband

3. Adequate reduction of overall filter structure size to achieve high degree of miniaturisation

The criterian for selection of parameters a and d are based on computation of unloaded quality factor (Q_0) and on spurious resonances. A good compromise between Q_0, spurious resonances and structure overall size may be achieved, with presently available dielectric materials, by choosing a and d in the range of values (for $\epsilon_d = 20 - 40$) [22]:-

$$0.5\, a_{max} \leq a \leq 0.6\, a_{max}$$
$$\frac{1.1}{\sqrt{\epsilon_d}}\, a_{max} \leq d \leq \frac{1.3}{\sqrt{\epsilon_d}}\, a_{max} \tag{6.2}$$

6.3 Filter Synthesis

Bandpass filter synthesis is usually started by designing a prototype lowpass lumped element network, using the insertion loss method. This lowpass prototype design has been the basis of design for a vast majority of filter [3, 23]. In insertion loss method, the design of the filter starts with the specifications about the insertion loss or the return loss for a lossless network, in the desired frequency band. After specifying the magnitude of the insertion loss as a function of frequency in the passband (Butterworth function, Chebycheve function etc.) the prototype values are obtained from the formulas given in [23]. Having obtained these prototype values the low
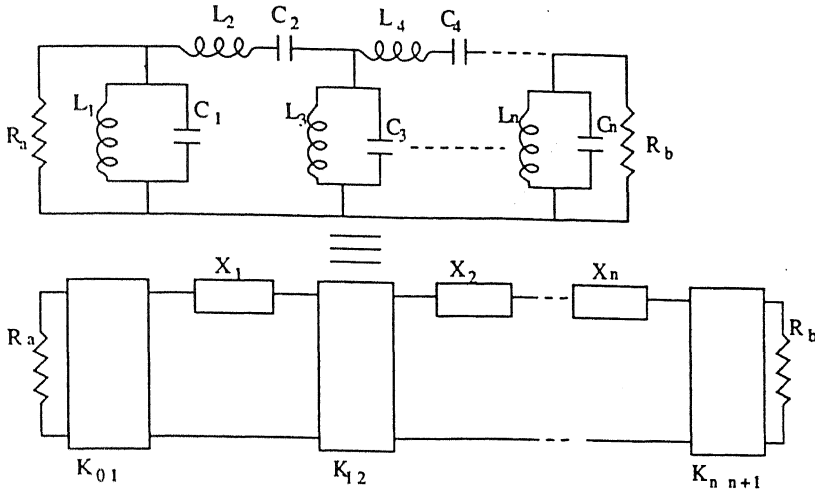
Figure 6.2: Equivalent circuit representation of direct coupled bandpass filter.

pass characteristic is transformed into bandpass characteristic by using well known lowpass to bandpass mapping.

Bandpass filter which are physically symmetric can be realized as a simple combination of resonators. For such filter (excluding the generalised filter which uses cross coupling amongst resonators) Matthaei[23] has given an equivalent circuit shown in the Fig 6.2. Input and output couplings for this circuit is represented by external quality factors $Q_{ext(a)}$ and $Q_{ext(b)}$ while coupling between resonators is represented by coupling coefficient $k_{j,j+1}$. These quantities are calculated in terms of low-pass prototype g_{is} values from the formula given below

$$
\begin{aligned}
Q_{ext(a)} &= \frac{X_1}{\left(K_{0,1}^2/R_a\right)} = \frac{g_0 g_1}{w} \\
Q_{ext(b)} &= \frac{X_n}{\left(K_{n,n+1}^2/R_b\right)} = \frac{g_n g_{n+1}}{w} \\
k_{j,j+1} &= \frac{K_{j,j+1}}{\sqrt{X_j X_{j+1}}} = \frac{w}{\sqrt{g_j g_{j+1}}} \quad j = 1, 2, 3 \ldots n-1
\end{aligned} \tag{6.3}
$$

here, w is the fractional bandwidth given by

$$w = \frac{w_2 - w_1}{w_0}$$
$$w_0 = \sqrt{w_2 \, w_1} \tag{6.4}$$

The passband edges w_2 and w_1, are for Chebycheve response, defined by pass-band ripple level. With Q_{ext} and k computed, design data are generated to relate these values to the electrical and physical parameters of the resonators and the inter-element spacing between them. This completes the synthesis of bandpass filter.

6.4 Proposed Filter Design and it's Specifications

Filter structure as shown in Fig 6.1 was concieved for design with the following specifications :-

1. Response : Chebychev response with 0.5 dB ripple in passband

2. Resonance frequency = 11.83 GHz

3. 3 dB bandwidth = ±50 Mhz

4. Stopband attenuation = 45 dB

On choosing disc type resonator and selecting the parameters a and d as per the previous section, following electrical and physical parameters of DRs are chosen :-

Height $2h = 4.04$mm

Diameter $2d = 7.27$mm

Dielectric constant of DR $\epsilon_d = 24.0$

Unloaded Quality factor $Q_0 = 25000$

For these specifications the design data obtained is as follows :-

Number of Resonators = 4

$g_0 = 1.0 \qquad g_1 = 1.6703$

$g_2 = 1.1926 \qquad g_3 = 2.3661$

$g_4 = 0.8419 \qquad g_5 = 1.9841$

$$Q_{ext(a)} = \frac{g_0 g_1}{\omega} = 197.59$$

$$Q_{ext(b)} = \frac{g_4 g_5}{\omega} = 197.6$$

$$k_{1,2} = \frac{\omega}{\sqrt{g_1 g_2}} = 5.989 \times 10^{-3}$$

$$k_{2,3} = \frac{\omega}{\sqrt{g_2 g_3}} = 5.032 \times 10^{-3}$$

$$k_{3,4} = \frac{\omega}{\sqrt{g_3 g_4}} = 5.989 \times 10^{-3}$$

$$(6.5)$$

The design charts for inter-resonator coupling for the DR specifications chosen above, are given in Figs 6.3 for $k_{1,2}$, $k_{3,4}$ and in Fig 6.4 for $k_{2,3}$, keeping substrate thickness equal to 7.65mm. However the values of Q_{exta} and Q_{extb} will have to be found by measurement, as their formulation could not be done due to time constraint and complexity involved.
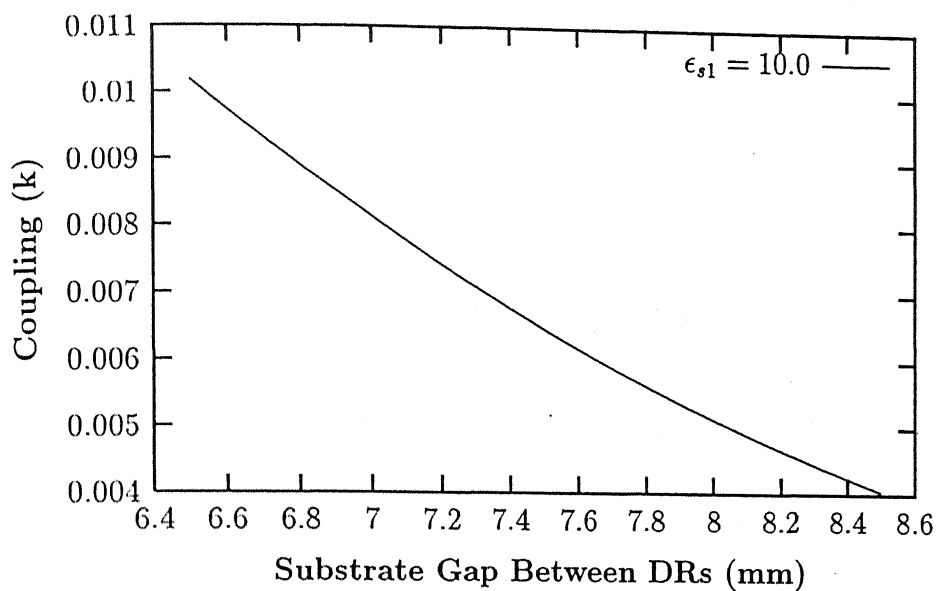
Figure 6.3: Variation of inter-resonator coupling through substrate
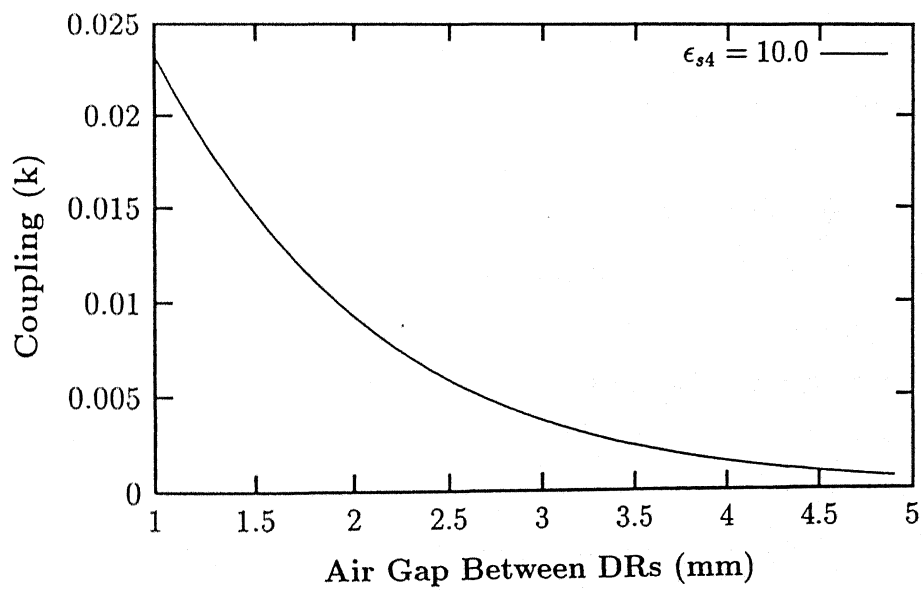
Figure 6.4: Variation of inter-resonator coupling through air

Chapter 7

Conclusion and Future Developments

7.1   Conclusion

The characteristics of Dielectric Resonator operating in $TM_{01\delta}$ mode has been studied in detail in various useful environments like Isolated cases, Post case, in cavity made of PEC/PMC circular plates, MIC enviroment, Suspended substrate environment and DR placed in a cylindrical waveguide below cutoff. The design parameters like resonance frequency, field configurations, energy distributions, computation of overall unloaded Q-factors, coupling between two resonators have been presented. The complete analysis is based on simple and approximate DWM method which gives reasonably accurate results, especially for DR post and Isolated DR. However, it was observed that pure DWM method gives high results for resonance frequency for close proximities of PEC surface, whereas for very close distances Modified DWM approach is more accurate. As the distance of PEC surface is increased, EDC approach with little modification gives reasonable accurate results. The energy distribution and computation of unloaded Q-factor has

been done using basic formulations. The effect of various structural parameters on resonance frequency, energy distribution, Q-factor and inter-resonator coupling have been discussed in detail. Interestingly, the substrate dielectric constant which does not affect the resonance frequency so much, plays an important role in electric energy distribution in various regions of the structure, and thereby it affects the quality factor and inter-resonator coupling tremendously.

Effective user friendly software packages have been developed using the above analysis which can be used for CAD of microwave circuits like filters, oscillators etc. The generated results have been compared with the available published data.

7.2   Future Developments

The behaviour of resonance frequency for close proximities of PEC surfaces can further be analysed in order to obtain accurate formulation covering PEC plate distance from post case to isolated case. The input and output couplings are required to be formulated, and thereafter practical realisation of proposed filter structure can be carried out. $TM_{01\delta}$ mode in suspended substrate environment, has rarely been reported and therefore it's applications in microwave circuit designs may be analysed further.

Bibliography

[1] J.K. Plourde and Chung-li Ren, "Application of Dielectric Resonators in Microwave Components", *IEEE Trans. Microwave Theory Tech.* vol MTT-29, pp 754-770,August 1981.

[2] D Kajfez and P Guillon, *"Dielectric Resonators"*, Artec House, Norwood MA, 1986.

[3] S.B. Cohn, "Microwave Bandpass Filters Containing High-Q Dielectric Resonators", *IEEE Trans. Microwave Theory Tech.* vol MTT-16, pp 218-227, April 1968.

[4] T. Itoh and R.S. Rudokas, "New Method for Computing the Resonant Frequencies of Dielectric Desonators", *IEEE Trans. Microwave Theory Tech.* vol MTT-25, pp 52-54, Jan 1977.

[5] S.W. Chen, K.A. Zaki and R. West, "Tunable Temperature Compensated Dielectric Resonators and Filters", *IEEE Trans. Microwave Theory Tech.* vol MTT-38, pp 1046-1049, August 1990.

[6] Rajiv Kumar Shukla, "Studies on Dielectric Resonator in Suspended Substrate Environment for Millimetric Wave Applications", *M.Tech. thesis*, Dept of Elect. Engg., I.I.T., Kanpur, Feb 1995.

[7] R.K. Mongia, "Resonant Frequency of Cylindrical Dielectric Resonator Placed in an MIC Environment", *IEEE Trans. Microwave Theory Tech.* vol MTT-38, pp 802-805, June 1990.

[8] K.A. Zaki, C. Chen, "Loss Mechanism in Dielectric Loaded Resonators", *IEEE Trans. Microwave Theory Tech.* vol MTT-33, pp 1448-1452, December 1985.

[9] M. Taheri and D. Mirshekhar Syahkal, "Accurate Determination of Modes in Dielectric Cylindrical Cavities Using a One Dimentional Finite Element Method", *IEEE Trans. Microwave Theory Tech.* vol MTT-37, pp1536-1541, October 1989.

[10] M. Tsuji, H Shigesava, K Takiyama, "Analytical and Experimental Investigations on Several Resonant Modes in Open Dielectric resonators", *IEEE Trans. Microwave Theory Tech* vol MTT-32, pp 628-633, June 1984.

[11] W Zheng, "Computation of Complex Resonance Frequencies of Isolated Composit Objects", *IEEE Trans. Microwave Theory Tech* vol MTT-37, pp 953-961, June 1989.

[12] A.W. Glisson, D. Kajfez, J. James, "Evaluation of Modes in Dielectric Resonator using Surface Integral Equation Formulation", *IEEE Trans. Microwave Theory Tech.* vol MTT-31, pp1023-1029, December 1983.

[13] A. Bermudez, P.Y. Guillon, "Application of Variational Principle for Calculation of Resonant Frequencies of Cylindrical Dielectric Resonators", *Electronic letters* vol 22 No1, pp 31-33, January 1986.

[14] R.K. Mongia, C.L. Larose, P. Bhartia, "Accurate Measurement of Q-factors of Isolated Dielectric Resonators", *IEEE Trans. Microwave Theory Tech* vol MTT-42, pp 1463-1466, August 1994.

[15] P.H. Harms, J.F. Lee, "A study of non-orthogonal FDTD Method versus the Conventional FDTD Technique for computing Resonant frequencies of Cylindrical Cavities", *IEEE Trans Microwave Theory Tech* vol MTT-40, pp 741-746, April 1992.

[16] Y. Kobayashi, M. Minegishi, "A Low Loss Bandpass Filter Using Electrically Coupled High-Q $TM_{01\delta}$ Dielectric Rod Resonators", *IEEE Trans. Microwave Theory Tech* vol MTT-36, pp 1727-1732, December 1988.

[17] D. Kajfez, "Incremental Frequency Rule for Computing the Q-factor of Shielded TE_{0mp} Dielectric Resonator", *IEEE Trans. Microwave Theory Tech* vol MTT-32, pp 941-943, August 1984.

[18] Pavan Kumar, "Experimental Procedure for Determination of Q_u, Q_{ext}, Q_L and Coupling of Dielectric Resonator and Development of DR Oscillator", *M.Tech. thesis*, Dept of Elect. engg., July 1996.

[19] P. Skalicky, "Direct Coupling Between two Dielectric Resonators", *Electronic Letters*, pp 332-334, April 1982.

[20] B. Byzery, P. Guillon, "$TM_{0\gamma\delta}$ Mode of Cylindrical Dielectric Resonators Applications to Microwave Filters", *IEEE MTT-S Dig. Microwave Symposium* 1985.

[21] Y. Kobayashi, M. Minegishi, "Precise Design of a Bandpass Filter using high-Q Dielectric Ring Resonator", *IEEE Trans. Microwave Theory Tech* vol MTT-35, pp1156-1160, December 1987.

[22] G. Macchiarella and G.B. Stracca, "An Accurate Design Approach for TM Mode Dielectric Resonator Filters in Circular Waveguide Below Cutoff", *IEEE Trans. Microwave Theory Tech* vol MTT-36, pp1321-1328, July 1994.

[23] L Young, G L Matthaei and E Jones, "Microwave Filters, Impedance Matching Networks and Coupling Structures", Mc-Graw Hill, 1965.

[24] X P Liang, K A Zaki, " Modelling of Cylindrical Dielectric Resonators in rectangular Waveguide and Cavities", *IEEE Trans. Microwave Theory Tech.* vol MTT-41, pp 2174-2181, December 1993.

Appendix A

Six Regions Structure

A.1 Values of Field Constants B_{is}

$$B = \frac{K_0\left(k_a a\right)}{I_0\left(k_a a\right)} \tag{A.1}$$

$$B_1 = \frac{\beta_1 \left[\begin{array}{c} \coth\left(\alpha_a h_2\right) \\ \tanh\left(\alpha_a h_2\right) \end{array} \right] \tan\left(\beta_1 h\right) - \epsilon_d \alpha_a}{\beta_1 \left[\begin{array}{c} \coth\left(\alpha_a h_2\right) \\ \tanh\left(\alpha_a h_2\right) \end{array} \right] + \epsilon_d \alpha_a \tan\left(\beta_1 h\right)} \tag{A.2}$$

$$B_2 = \frac{\epsilon_d \left\{ \cos\left(\beta_1 h\right) + B_1 \sin\left(\beta_1 h\right) \right\}}{e^{-\alpha_a h_4} \left[\begin{array}{c} \cosh\left(\alpha_a h_2\right) \\ \sinh\left(\alpha_a h_2\right) \end{array} \right]} \tag{A.3}$$

$$B_3 = \frac{\epsilon_d \left\{ \cos\left(\beta_1 h\right) - B_1 \sin\left(\beta_1 h\right) \right\}}{\epsilon_s e^{-\alpha_s h_3} \left[\begin{array}{c} \cosh\left(\alpha_s h_1\right) \\ \sinh\left(\alpha_s h_1\right) \end{array} \right]} \tag{A.4}$$

$$B_5 = B_2 \cdot B_6 \tag{A.5}$$

$$B_6 = \frac{J_0\left(k_r d\right)}{K_0\left(k_a d\right) - B \, I_0\left(k_a d\right)} \tag{A.6}$$

$$B_7 = B_3 \cdot B_6 \tag{A.7}$$

where,

$$h_4 = h + h_2 \tag{A.8}$$

$$h_3 = h + h_1 \tag{A.9}$$

A.2 A_{ijs} and t Terms

$$A_{16} = \int_{-h}^{h} \{\cos{(\beta_1 z)} + B_1 \sin{(\beta_1 z)}\}^2 \ dz \tag{A.10}$$

$$= h \left\{ 1 + B_1^2 + \frac{\sin{(2\beta_1 h)}}{2\beta_1 h} \left(1 - B_1^2 \right) \right\} \tag{A.11}$$

$$A_{16'} = \int_{-h}^{h} \{\sin{(\beta_1 z)} - B_1 \cos{(\beta_1 z)}\}^2 \ dz \tag{A.12}$$

$$= h \left\{ 1 + B_1^2 - \frac{\sin{(2\beta_1 h)}}{2\beta_1 h} \left(1 - B_1^2 \right) \right\} \tag{A.13}$$

$$t_{(h_2,h_4,\alpha_a)} = e^{-2\alpha_a h_4} \int_{h}^{h_4} \sinh^2{\{\alpha_a (z - h_4)\}} \ dz \tag{A.14}$$

$$= \frac{\sinh{(2\alpha_a h_2)} - 2\alpha_a h_2}{4 \ \alpha_a \ e^{2\alpha_a h_4}} \tag{A.15}$$

$$t'_{(h_2,h_4,\alpha_a)} = e^{-2\alpha_a h_4} \int_{h}^{h_4} \cosh^2{\{\alpha_a (z - h_4)\}} \ dz \tag{A.16}$$

$$= \frac{\sinh{(2\alpha_a h_2)} + 2\alpha_a h_2}{4 \ \alpha_a \ e^{2\alpha_a h_4}} \tag{A.17}$$

$$t_{(h_1,h_3,\alpha_s)} = e^{-2\alpha_s h_3} \int_{-h_3}^{-h} \sinh^2{\{\alpha_s (z + h_3)\}} \ dz \tag{A.18}$$

$$= \frac{\sinh{(2\alpha_s h_1)} - 2\alpha_s h_1}{4 \ \alpha_s \ e^{2\alpha_s h_3}} \tag{A.19}$$

$$t'_{(h_1,h_3,\alpha_s)} = e^{-2\alpha_s h_3} \int_{-h_3}^{-h} \cosh^2{\{\alpha_s (z + h_3)\}} \ dz \tag{A.20}$$

$$= \frac{\sinh{(2\alpha_s h_1)} + 2\alpha_s h_1}{4 \ \alpha_s \ e^{2\alpha_s h_3}}$$

Appendix B

Integrals involving Bessel Functions

$$I_{JO} = \int_0^d r\, J_0^2(k_r r)\; dr$$

$$= \frac{d^2}{2} \left\{ J_1^2(k_r d) + J_0^2(k_r d) \right\} \tag{B.1}$$

$$I_{EJ} = \int_0^d r\, J_1^2(k_r r)\; dr$$

$$= \frac{d^2}{2} \left\{ J_1^2(k_r d) + J_0^2(k_r d) - \frac{2}{k_r d} J_0(k_r d) \cdot J_1(k_r d) \right\} \tag{B.2}$$

$$I_{KIO} = \int_d^a r\, \left\{ K_0(k_a r) - B\, I_0(K_a r) \right\}^2\; dr$$

$$= \left[\frac{r^2}{2} \left\{ K_1^2(k_a r) - K_0^2(k_a r) \right\} \right]_a^d + B^2 \left[\frac{r^2}{2} \left\{ I_0^2(k_a r) - I_1^2(k_a r) \right\} \right]_d^a$$

$$- B \left[r^2 \left\{ I_0(k_a r) K_0(k_a r) + I_1(k_a r) K_1(k_a r) \right\} \right]_d^a \tag{B.3}$$

$$I_{EKI} = \int_d^a r\, \left\{ K_1(k_a r) + B\, I_1(K_a r) \right\}^2\; dr$$

$$= \left[\frac{r^2}{2} \left\{ K_0^2(k_a r) - K_1^2(k_a r) + \frac{2}{k_a r} K_0(k_a r) \cdot K_1(k_a r) \right\} \right]_a^d$$

$$+ B^2 \left[\frac{r^2}{2} \left\{ I_0^2(k_a r) - I_1^2(k_a r) - \frac{2}{k_a r} I_0(k_a r) \cdot I_1(k_a r) \right\} \right]_a^d$$

$$+ B \left[r^2 \left\{ I_0(k_a r) K_0(k_a r) + \frac{2}{(k_a r)} I_0(k_a r) K_1(k_a r) + I_1(k_a r) K_1 \right. \right.$$

$$I_{KO} = \int_0^{2\pi} \int_0^d J_0\left(k_r r\right) \left\{K_0\left(k_a r'\right) - B\, I_0\left(k_a r'\right)\right\} \frac{r\left\{r + (2d + S)\sin\phi\right\}}{r'} \, dr \, d\phi$$

$$(B.4)$$

where,

$$r' = \left[\, r^2 + (2d + S)^2 + 2\,(2d + S)\, r \sin\phi \,\right]^{1/2} \tag{B.5}$$

This integral is evalvated using Nag subroutines (D01DAF).

Appendix C

Ten Regions Structure

C.1 Values of field Constants B_{is}

$$B = \frac{K_0(k_a a)}{I_0(k_a a)} \tag{C.1}$$

$$B_1 = \frac{\epsilon_d \beta_2 + \epsilon_{s4} m_3 \tan(\beta_1 h)}{\epsilon_{s4} \beta_1 m_3 - \epsilon_d \beta_2 \tan(\beta_1 h)} \tag{C.2}$$

$$B_2 = \frac{\beta_1 \{ B_1 \cos(\beta_1 h) - \sin(\beta_1 h) \}}{\beta_2 \{ B_3 \cos(\beta_2 h) - \sin(\beta_2 h) \}} \tag{C.3}$$

$$B_3 = \frac{m_1 \tan(\beta_2 h_5) - 1.0}{m_1 + \tan(\beta_2 h_5)} \tag{C.4}$$

$$B_4 = -B_2 \cdot \frac{\beta_2 \{ B_3 \cos(\beta_2 h_5) - \sin(\beta_2 h_5) \}}{\alpha_{s3} e^{-\alpha_{s3} h_6} \left[\begin{array}{c} \sinh(\alpha_{s3} h_4) \\ \cosh(\alpha_{s3} h_4) \end{array} \right]} \tag{C.5}$$

$$B_5 = \frac{\beta_1 \{ B_1 \cos(\beta_1 h) + \sin(\beta_1 h) \}}{\beta_3 \{ B_6 \cos(\beta_3 h) + \sin(\beta_3 h) \}} \tag{C.6}$$

$$B_6 = \frac{1.0 - m_2 \tan(\beta_3 h_7)}{m_2 + \tan(\beta_3 h_7)} \tag{C.7}$$

$$B_7 = B_5 \cdot \frac{\beta_3 \{ B_6 \cos(\beta_3 h_7) + \sin(\beta_3 h_7) \}}{\alpha_{s2} e^{-\alpha_{s2} h_8} \left[\begin{array}{c} \sinh(\alpha_{s2} h_3) \\ \cosh(\alpha_{s2} h_3) \end{array} \right]} \tag{C.8}$$

$$B_8 = B_4 \cdot B_{10} \tag{C.9}$$

$$B_9 = B_2 \cdot B_{10} \tag{C.10}$$

$$B_{10} = \frac{J_0(k_r d)}{K_0(k_a d) - B\,I_0(k_a d)} \tag{C.11}$$

$$B_{11} = B_5 \cdot B_{10} \tag{C.12}$$

$$B_{12} = B_7 \cdot B_{10} \tag{C.13}$$

where,

$$h_5 = h + h_2 \tag{C.14}$$

$$h_6 = h + h_2 + h_4 \tag{C.15}$$

$$h_7 = h + h_1 \tag{C.16}$$

$$h_8 = h + h_1 + h_3 \tag{C.17}$$

C.2 A_{ijs} and t Terms

$$A_{16} = \int_{-h}^{h} \{\cos(\beta_1 z) + B_1 \sin(\beta_1 z)\}^2 \, dz \tag{C.18}$$

$$= h \left\{ 1 + B_1^2 + \frac{\sin(2\beta_1 h)}{2\beta_1 h} \left(1 - B_1^2\right) \right\} \tag{C.19}$$

$$A_{16'} = \int_{-h}^{h} \{\sin(\beta_1 z) - B_1 \cos(\beta_1 z)\}^2 \, dz \tag{C.20}$$

$$= h \left\{ 1 + B_1^2 - \frac{\sin(2\beta_1 h)}{2\beta_1 h} \left(1 - B_1^2\right) \right\} \tag{C.21}$$

$$A_{17} = \int_{h}^{h_5} [B_2 \{\cos(\beta_2 z) + B_3 \sin(\beta_2 z)\}] \cdot [B_2 \{\cos(\beta_2 z) + B_3 \sin(\beta_2 z)\}]^* \, dz \tag{C.22}$$

(i)   If B_2, B_3, β_2 are all Real, OR β_2, B_3 Real and B_2 Imaginary then

$$A_{17} = \frac{1}{2} B_2^2 h_2 [1 + B_3^2 + \frac{\sin(\beta_2 h_2)}{\beta_2 h_2} \{(1 - B_3^2) \cos\{\beta_2(2h + h_2)\} + \\ 2B_3 \sin\{\beta_2(2h + h_2)\}] \tag{C.23}$$

(ii) If B_2, B_3 Real, and β_2 Imaginary OR B_3 Real and β_2, B_2 Imaginary then

$$A_{17} = \frac{1}{2}B_2^2h_2[1 - B_3^2 + \frac{\sinh(\beta_2h_2)}{\beta_2h_2}\{(1 + B_3^2)\cosh\{\beta_2(2h + h_2)\}\}]$$

(C.24)

(iii) If β_2, B_2 Real, and B_3 Imaginary OR β_2 Real and B_2, B_3 Imaginary then

$$A_{17} = \frac{1}{2}B_2^2h_2[1 + B_3^2 + \frac{\sin(\beta_2h_2)}{\beta_2h_2}\{(1 - B_3^2)\cos\{\beta_2(2h + h_2)\}\}] \quad (C.25)$$

(iv) If B_2 Real, and β_2, B_3 Imaginary OR β_2, B_2, B_3 are all Imaginary then

$$A_{17} = \frac{1}{2}B_2^2h_2[1 - B_3^2 + \frac{\sinh(\beta_2h_2)}{\beta_2h_2}\{(1 + B_3^2)\cosh\{\beta_2(2h + h_2)\} -$$
$$2B_3\sinh\{\beta_2(2h + h_2)\}] \quad (C.26)$$

$$A'_{17} = \int_h^{h_5}[B_2\beta_2\{B_3\cos(\beta_2z) - \sin(\beta_2z)\}] \cdot [B_2\beta_2\{B_3\cos(\beta_2z) - \sin(\beta_2z)\}]^* \, dz$$

(C.27)

(i) If B_2, B_3, β_2 are all Real, OR β_2, B_3 Real and B_2 Imaginary then

$$A'_{17} = \frac{1}{2}B_2^2\beta_2^2h_2[1 + B_3^2 - \frac{\sin(\beta_2h_2)}{\beta_2h_2}\{(1 - B_3^2)\cos\{\beta_2(2h + h_2)\} +$$
$$2B_3\sin\{\beta_2(2h + h_2)\}] \quad (C.28)$$

(ii) If B_2, B_3 Real, and β_2 Imaginary OR B_3 Real and β_2, B_2 Imaginary then

$$A'_{17} = \frac{1}{2}B_2^2\beta_2^2h_2[B_3^2 - 1 + \frac{\sinh(\beta_2h_2)}{\beta_2h_2}\{(1 + B_3^2)\cosh\{\beta_2(2h + h_2)\}\}]$$

(C.29)

(iii)   If β_2, B_2 Real, and B_3 Imaginary OR β_2 Real and B_2, B_3 Imaginary then

$$A'_{17} = \frac{1}{2}B_2^2\beta_2^2 h_2[1 + B_3^2 + \frac{\sin(\beta_2 h_2)}{\beta_2 h_2}\{(B_3^2 - 1)\cos\{\beta_2(2h + h_2)\}\}]$$

$$(C.30)$$

(iv)   If B_2 Real, and β_2, B_3 Imaginary OR β_2, B_2, B_3 are all Imaginary then

$$A'_{17} = \frac{1}{2}B_2^2\beta_2^2 h_2[B_3^2 - 1 + \frac{\sinh(\beta_2 h_2)}{\beta_2 h_2}\{(1 + B_3^2)\cosh\{\beta_2(2h + h_2)\} - 2B_3\sinh\{\beta_2(2h + h_2)\}]$$

$$(C.31)$$

Note :- Here only neumerical values of real or imaginary parts of B_2, B_3 and β_2 are to be substituted.

$$A_{18} = \int_{-h_7}^{-h} [B_5\{\cos(\beta_3 z) + B_6\sin(\beta_3 z)\}] \cdot [B_5\{\cos(\beta_3 z) + B_6\sin(\beta_3 z)\}]^* \ dz$$

$$A'_{18} = \int_{-h_7}^{-h} [B_5\beta_3\{B_6\cos(\beta_3 z) - \sin(\beta_3 z)\}] \cdot [B_5\beta_3\{B_6\cos(\beta_3 z) - \sin(\beta_3 z)\}]^* \ dz$$

$$(C.32)$$

Values of these integrals can be obtained by replacing B_2 by B_5, B_3 by B_6, β_2 by β_3 and h_2 by h_1 in the values of A_{17} and A'_{17} with signs of last two terms reversed in case (i) and (iv).

$$t_{(h_4,h_6,\alpha_{s3})} = e^{-2\alpha_{s3}h_6} \int_{h_5}^{h_6} \sinh^2\{\alpha_{s3}(z - h_6)\} \ dz \qquad (C.33)$$

$$= \frac{\sinh(2\alpha_{s3}h_4) - 2\alpha_{s3}h_4}{4\ \alpha_{s3}\ e^{2\alpha_{s3}h_6}} \qquad (C.34)$$

$$t'_{(h_4,h_6,\alpha_{s3})} = e^{-2\alpha_{s3}h_6} \int_{h_5}^{h_6} \cosh^2\{\alpha_{s3}(z - h_6)\} \ dz \qquad (C.35)$$

$$= \frac{\sinh(2\alpha_{s3}h_4) + 2\alpha_{s3}h_4}{4\ \alpha_{s3}\ e^{2\alpha_{s3}h_6}} \qquad (C.36)$$

$$t_{(h_3,h_8,\alpha_{s2})} = e^{-2\alpha_{s2}h_8} \int_{-h_8}^{-h_7} \sinh^2\{\alpha_{s2}(z + h_8)\} \ dz \qquad (C.37)$$

81

$$= \frac{\sinh(2\alpha_{s2}h_3) - 2\alpha_{s2}h_3}{4\,\alpha_{s2}\,e^{2\alpha_{s2}h_8}} \tag{C.38}$$

$$t'_{(h_3,h_8,\alpha_{s2})} \doteq e^{-2\alpha_{s2}h_8} \int_{-h_8}^{-h_7} \cosh^2\{\alpha_{s2}(z+h_8)\}\,dz \tag{C.39}$$

$$= \frac{\sinh(2\alpha_{s2}h_3) + 2\alpha_{s2}h_3}{4\,\alpha_{s2}\,e^{2\alpha_{s2}h_8}} \tag{C.40}$$

$$A'_{19} = \int_{-h}^{h} \{\cos(\beta_1 z) - B_1\sin(\beta_1 z)\}\cdot\sinh\{\alpha_{s2}(h_3 - h + z)\}\,dz$$
$$= \frac{1}{\beta_1^2 + \alpha_{s2}^2}\,[\,\beta_1\sin(\beta_1 h)\,\{\sinh(\alpha_{s2}h_3) + \sinh\{\alpha_{s2}(h_3 - 2h)\}\} +$$
$$\alpha_{s2}\cos(\beta_1 h)\,\{\cosh(\alpha_{s2}h_3) - \cosh\{\alpha_{s2}(h_3 - 2h)\}\} -$$
$$B_1\,\{\beta_1\cos(\beta_1 h)\,\{\sinh\{\alpha_{s2}(h_3 - 2h)\} - \sinh(\alpha_{s2}h_3\} +$$
$$\alpha_{s2}\sin(\beta_1 h)\,\{\cosh\{\alpha_{s2}(h_3 - 2h)\} + \cosh(\alpha_{s2}h_3\}\,\}] \tag{C.41}$$